# NATIONAL ADVISORY COMMITTEE FOR AERONAUTICS

TECHNICAL NOTE 4041

THE SUBSONIC STATIC AERODYNAMIC CHARACTERISTICS OF AN AIRPLANE MODEL HAVING A TRIANGULAR WING OF ASPECT RATIO 3. I - EFFECTS OF HORIZONTAL-TAIL LOCATION AND SIZE ON THE LONGITUDINAL CHARACTERISTICS

By Bruce E. Tinling and Armando E. Lopez

Ames Aeronautical Laboratory Moffett Field, Calif.



Washington
July 1957

#### NATIONAL ADVISORY COMMITTEE FOR AERONAUTICS

## TECHNICAL NOTE 4041

THE SUBSONIC STATIC AERODYNAMIC CHARACTERISTICS OF AN AIRPLANE MODEL HAVING A TRIANGULAR WING OF ASPECT RATIO 3. I - EFFECTS OF HORIZONTAL-TAIL LOCATION AND SIZE ON THE LONGITUDINAL CHARACTERISTICS 1

By Bruce E. Tinling and Armando E. Lopez

#### SUMMARY

An investigation has been conducted to determine the effects of horizontal-tail location and size on the longitudinal aerodynamic characteristics of an airplane model having a triangular wing. The wing had an aspect ratio of 3 and the NACA 0003.5-63 section in the streamwise direction. Two horizontal tails were tested which had areas of either 16.7 or 21.9 percent of the wing area. Each of the horizontal tails had an aspect ratio of 4, a taper ratio of 0.33, the NACA 0004-64 section, and no sweepback of the 50-percent-chord line. Tests were conducted with the horizontal tails located -0.10, 0, 0.10, and 0.20 wing semispans above the chord plane of the wing at longitudinal distances of 1.2 and 1.5 mean aerodynamic chord lengths behind the moment center. The wind-tunnel tests were conducted at a Reynolds number of 2.5 million at Mach numbers from 0.25 to 0.95.

It was found that the horizontal tail was destabilizing at moderate lift coefficients when located above the plane of the wing. When placed either in or below the plane of the wing, the horizontal tail was stabilizing throughout the lift range. For the balanced condition, the drag increment due to the tail was less when the tail was placed 0.10 wing semispan below the wing chord plane than when placed in the wing chord plane. In general, the drag due to balancing the model decreased with increases in tail size or length and increased markedly as the Mach number was increased beyond 0.90.

## INTRODUCTION

The subsonic aerodynamic characteristics of a model of an airplane having a triangular wing of aspect ratio 3 and an all-movable horizontal tail have been the subject of an investigation in the Ames 12-foot pressure wind tunnel. Results obtained during this investigation which pertain to the static lateral and directional characteristics and to the effects

<sup>&</sup>lt;sup>1</sup>Supersedes recently declassified NACA RM A53L15 by Bruce E. Tinling and Armand E. Lopez, 1954.

of trailing-edge flaps are reported in references 1 and 2. Ground effects on the longitudinal characteristics are reported in reference 3.

This report presents a part of the investigation undertaken to determine the effects of longitudinal and vertical position and of size of the horizontal tail on the static longitudinal characteristics. The effects of vertical position of the horizontal tail on the low-speed characteristics of a similar configuration have been reported in reference 4, and a study of the downwash at transonic speeds behind a triangular wing having an aspect ratio of 3 has been presented in reference 5. The wind-tunnel tests of the present investigation were conducted at Mach numbers up to 0.95 at a Reynolds number of 2.5 million, and at Reynolds numbers of 2.5 million and 10 million at a Mach number of 0.25.

## NOTATION

A	aspect ratio, $\frac{b^2}{S}$
a	normal acceleration
b	wing span
$c_{\mathrm{D}}$	drag coefficient, drag qS
$\Delta c_{\mathrm{D}_{\mathrm{otail}}}$	$C_{\text{Dtail on}}$ - $C_{\text{Dtail off}}$ , measured at $\alpha$ = 0 and it $\approx$ 0
$c_{\mathbf{L}}$	lift coefficient, lift qS
C <sub>m</sub>	pitching-moment coefficient about the moment center,  pitching moment  qSc
С	wing chord measured parallel to the plane of symmetry
	Wing chord measured paraffer to the praise of symmetry
ē	wing mean aerodynamic chord, $\frac{2}{S_W} \int_0^{b/2} c^2 dy$
īc g	
	wing mean aerodynamic chord, $\frac{2}{S_W} \int_0^{b/2} c^2 dy$

the horizontal-tail pivot line

L D	lift-drag ratio, lift drag
M	free-stream Mach number
n	normal acceleration factor, $\frac{a}{g}$
q	free-stream dynamic pressure
R	Reynolds number, based on the wing mean aerodynamic chord
St	area of the horizontal tail
$S_{\overline{W}}$	wing area
V <sub>h</sub>	tail volume, $\frac{l_t}{\bar{c}} \frac{S_t}{S_w}$
У	lateral distance from the plane of symmetry
Z	vertical distance from the wing chord plane to the hinge axis of the horizontal tail
α	angle of attack, deg
€	effective downwash angle, deg
$\frac{\partial c_m}{\partial i_t}$	horizontal-tail pitching-moment effectiveness, measured at a constant angle of attack
$\eta\left(\frac{q_{t}}{q}\right)$	tail-efficiency factor (ratio of the lift-curve slope of the horizontal tail when mounted on the fuselage in the flow field of the wing to the theoretical lift-curve slope of the isolated horizontal tail evaluated by the method of reference 6)

#### MODEL

The triangular wing of the model tested during this investigation had an aspect ratio of 3 and the NACA 0003.5-63 streamwise section. Two horizontal tails were tested which had areas of either 16.7 or 21.9 percent of the wing area. Each horizontal tail had an aspect ratio of 4, a taper ratio of 0.33, and the NACA 0004-64 streamwise section. The wing, tail surfaces, and fuselage were machined from solid steel. Further details of the geometry of components of the model are given in table I.

As shown in figure 1, both the horizontal tail and the wing could be placed on or above the fuselage center line. This permitted the horizontal-tail hinge line to be located at -0.10, 0, 0.10, or 0.20 wing semispans above the wing chord plane. A change in tail length was obtained by removing a cylindrical portion of the fuselage which was 6.50 inches in length. The moment center chosen for each combination of tail size and position and the corresponding tail lengths are tabulated in table II. As can be noted from table II, the tail sizes and lengths were chosen so that nearly the same tail volume could be obtained with either tail length.

The model was supported in the tunnel by a sting as shown in figure 2. A 4-inch-diameter, 4-component, strain-gage balance enclosed within the model body was used to measure the forces and moments.

## CORRECTIONS TO DATA

The data have been corrected for the induced effects of the tunnel walls resulting from lift on the model by the method of reference 7. The magnitudes of the corrections which were added to the measured values are:

$$\Delta \alpha = 0.30 \text{ C}_{\text{L}}$$

$$\Delta C_D = 0.0045 C_L^2$$

The induced effects of the tunnel walls on both the tail-on and tail-off pitching moments were calculated and found to be negligible.

Corrections to the data to account for the effects of constriction due to the tunnel walls were calculated by the method of reference 8. At a Mach number of 0.90, this correction amounted to an increase of about 1 percent in the dynamic pressure.

The effect of interference between the model and the sting support which could influence the measured forces and moments, particularly those due to the horizontal tail, is not known. It is believed that the main effect of the sting on the drag data was to alter the pressure at the base of the model body. Consequently, the pressure at the base of the model was measured and the drag data were adjusted to correspond to a base pressure equal to free-stream static pressure.

#### RESULTS AND DISCUSSION

The results of the wind-tunnel tests pertaining to longitudinal stability and control are presented in figures 3 through 20, and those pertaining to drag are presented in figures 21 through 25. It was convenient when evaluating the effects of tail size and position on the longitudinal aerodynamic characteristics to select the moment center for each configuration to yield the same static margin at some condition. Since the static longitudinal stability was the smallest at low speed, the moment center was selected to yield a static margin of 6 percent of the mean aerodynamic chord ( $dC_{\rm m}/dC_{\rm L} = -0.06$ ) at zero lift and zero tail incidence at a Mach number of 0.25. The resulting moment centers for the various combinations of tail size and location are listed in table II.

## Longitudinal Stability and Control Characteristics

Tail off.- The tail-off lift and pitching-moment coefficients measured during tests with the wing in the mid or in the high position are shown in figure 3. As would be anticipated from the results reported in reference 9, displacing the wing had no important effects on the lift or pitching-moment characteristics at moderate lift coefficients.

The longitudinal static stability of the wing-fuselage combination decreased as the lift coefficient was increased from about 0.2 to 0.5 at Mach numbers up to 0.90. Additional measurements were made to determine the Mach number at which this effect was the most severe. These additional data (fig. 4) indicate this reduction in longitudinal stability to have been the greatest at Mach numbers from 0.80 to 0.85.

At a Mach number of 0.95, the stability increased markedly as the lift coefficient was increased. Since this effect was opposite that which occurred at a Mach number of 0.90, a large increase in static margin resulted for moderate lift coefficients when the Mach number was increased from 0.90 to 0.95. This increase in static margin amounted to about 13 percent of the mean aerodynamic chord at a lift coefficient of 0.4. (See fig. 3.)

Effect of horizontal-tail position and size. The contribution of the horizontal tail to the pitching-moment-curve slope is approximately equal to

$$-\left(\frac{\text{St}}{\text{Sw}}\right)\left(\frac{l_{\text{t}}}{\bar{c}}\right)\left[\eta\left(\frac{q_{\text{t}}}{q}\right)\frac{\left(\text{dC}_{\text{L}}/\text{d}\alpha\right)_{\text{tail off}}}{\left(\text{dC}_{\text{L}}/\text{d}\alpha\right)_{\text{tail off}}}\left(1-\frac{\text{d}\varepsilon}{\text{d}\alpha}\right)\right]$$

The parameters within the brackets were found to have only small variations with tail size. The following discussion, therefore, is concerned mostly with the effects of tail height and tail length. The effect of tail size has been considered to be merely a geometric factor by which the control effectiveness and the contribution of the horizontal tail to the longitudinal stability may be varied. The values of the tail efficiency factor  $\eta(q_t/q)$  and the downwash  $\varepsilon$  were calculated from the following equations:

 $\epsilon = \alpha + i_t - \frac{\binom{C_m_{tail on} - C_m_{tail off}}{(\partial C_m/\partial i_t)}$ 

$$\eta \left(\frac{q_t}{q}\right) = \frac{\partial c_m / \partial i_t}{\left(dc_L / d\alpha\right)_{tail}}$$

It is assumed in this method that the lift curve of the horizontal tail is linear. Consequently,  $\varepsilon$  and  $\eta(q_{\pm}/q)$  were not calculated for angles of attack for which the data indicated that the tail might be stalled. The values of the lift-curve slope of the isolated horizontal tail used

in calculating the factors  $\frac{(dC_L/d\alpha)_{\mbox{tail}}}{(dC_L/d\alpha)_{\mbox{tail}}}$  and  $\eta(q_{\mbox{t}}/q)$  were calculated

by the method of reference 6.

The results in references 4 and 5 indicate the horizontal tail to be destabilizing for moderate lift coefficients when located 0.20 b/2 or 0.40 b/2 above the wing chord plane. The results of the present investigation (fig. 5) show that this effect, although reduced in magnitude, also occurred when the tail was 0.10 b/2 above the wing chord plane and was less severe with the greater tail length. At a Mach number of 0.95, the destabilizing effect of placing the tail above the wing chord plane was obscured since the reduction in the stability contribution of the tail with increasing lift coefficient was compensated by an increase in the stability contribution of the wing-fuselage combination. (See fig. 3.) As is shown in references 4 and 5, the adverse effect of increasing the tail height on the longitudinal stability was caused by differences in the variation of downwash at the tail with angle of attack. This cause is illustrated in figure 6 where the variations with lift coefficient of the tail contribution to the pitching-moment-curve slope and of the downwash factor

 $\left(1 - \frac{d\epsilon}{d\alpha}\right)$  are presented.

It is evident from the data of figures 5 and 6 that the horizontal tail was stabilizing throughout the lift range only when it was in either of the two lower positions  $\left(\frac{z}{b/2} = 0 \text{ and } \frac{z}{b/2} = -0.10\right)$ . Data obtained to evaluate the longitudinal stability and control characteristics at Mach numbers of 0.25, 0.60, 0.80, 0.90, 0.93, and 0.95 for most combinations of tail length and size for each of these tail heights are presented in figures 7 through 14. The average effective downwash calculated from these data for each tail location is presented in figure 15.

Inspection of the data of figures 7 through 14 indicates that the horizontal tail was effective as a longitudinal control for all combinations of tail size and position throughout the Mach number range. At low speed, it was possible to balance the model at a lift coefficient of about 1 with a tail incidence of about -8° for all configurations. A positive static margin was maintained at all Mach numbers with the exception of a region of marginal stability at a Mach number of 0.80 for a lift coefficient of approximately 0.4 for some combinations of horizontal tail size and location.

The variation with Mach number of the factors contributing to the longitudinal stability is presented in figure 16. From these data it can be seen that the change in  $dC_m/dC_L$  between Mach numbers of 0.25 and 0.95 was less with the tail on than with the tail off by between 0.02 and 0.04, depending upon the tail size and location. This effect can be traced to the diminishing value of the factor  $\left(1-\frac{d\varepsilon}{d\alpha}\right)$  with increasing Mach number. It can also be seen by comparing parts (a) and (b) of figure 16 that  $\left(1-\frac{d\varepsilon}{d\alpha}\right)$  was greater when the tail was in the lower position  $\left(\frac{z}{b/2}=-0.10\right)$ .

As noted previously, the longitudinal stability of the wing-fuselage combination diminished as the lift coefficient was increased from about 0.2 to 0.5 at Mach numbers up to 0.90. The pitching moment contributed by the tail when located in or below the wing chord plane varied with lift in a manner which tended to compensate for these undesirable tail-off characteristics. This is illustrated in figures 17 and 18 where the pitching-moment coefficient caused by the horizontal

tail per unit of tail volume and the factors  $\frac{(dC_L/d\alpha)_{tail}}{(dC_L/d\alpha)_{tail}}$  and

 $\left(1-\frac{d\varepsilon}{d\alpha}\right)$  have been presented. (The factor  $\eta\left(\frac{q_t}{q}\right)$  has not been presented since it was found to be invariant with lift coefficient.)

The Mach numbers of 0.25, where the static margin at zero lift was the least, and 0.80, where the tail-off pitching-moment variation tended to cause instability, have been chosen for this illustration. These data show that the stability contribution of the tail increased markedly as the lift coefficient was increased beyond about 0.3, particularly for the greater tail length. This accounts for the improved pitching-moment characteristics for the larger tail volumes, particularly when the horizontal tail was in the wing chord plane. (Cf. figs. 7(a) with 10(a) and 7(c) with 10(c).) The increased tail contribution to the stability for lift coefficients greater than about 0.3 was caused by increases in the

downwash factor  $\left(1-\frac{d\varepsilon}{d\alpha}\right)$  and to a lesser extent by decreases in the wing lift-curve slope as indicated by the variation of  $\frac{(dC_L/d\alpha)_{tail}}{(dC_L/d\alpha)_{tail}}$ .

(See figs. 17(b) and 18(b).) This increase in the stability contribution was not as great for the tails placed below the wing chord plane as for those placed in the wing chord plane. (See figs. 17(a) and 18(a).) However, at a Mach number of 0.80, the static margin at zero lift was from 1 to 3 percent greater with the tail in the lower position than with the tail in the wing chord plane. As a result, the minimum static margin (at  $C_L \approx 0.4$ ) was nearly the same for either of the tail positions at a Mach number of 0.80. (Cf. figs. 8(c) with 12(c), 9(c) with 13(c), and 10(c) with 14(c).)

Application of data. The data for the two lower tail positions were used to calculate the variation of tail incidence with Mach number for an airplane having a wing loading of 60 lb/ft² flying at an altitude of 30,000 feet. The results of these calculations are presented in figure 19. The variation of tail incidence with speed indicated stickfixed longitudinal stability up to a Mach number of about 0.90. However, with further increase in Mach number, the tail incidence required for balance became more negative. This apparent loss of longitudinal control effectiveness, which became more severe with increasing normal acceleration factor, was caused by increases with Mach number of the static margin, without corresponding increases of the pitching-moment effectiveness of the tail. The increase in static margin was caused by the increase in the stability of the wing-fuselage combination at moderate lift coefficients. (See fig. 3.)

Effect of Reynolds number. The results of tests conducted to evaluate the effects of Reynolds number on the low-speed lift and pitching-moment characteristics are presented in figure 20. A change in the Reynolds number from 2.5 million to 10 million had no important effect on the low-speed stability and control characteristics of the model when the wing and the tail were located on the fuselage center line. Similar results, not presented herein, were obtained from tests with the wing in the high position.

Lift and pitching-moment data presented in reference 6 show the effects of Reynolds number to be negligible between 3.1 and 4.8 million at Mach numbers from 0.6 to 0.9 for a wing of the same plan form, but with a thickness-chord ratio of 3 percent. The lift and pitching-moment data of reference 9 were found to be in excellent agreement with those of the present investigation when the moment center was selected to obtain identical static margins at zero lift.

### Drag Characteristics

Effect of Reynolds number. The drag coefficient and the lift-drag ratios measured during low-speed tests with the wing in the mid position at Reynolds numbers of 2.5 and 10 million are presented in figure 21. These data show that the drag due to lift was greater at the lower Reynolds number. The resulting difference in the maximum lift-drag ratio was about 12 percent. Similar results were obtained from tests with the wing in the high position.

Effect of wing position. The tail-off drag data are summarized in figures 22 and 23. In figure 22, three measured values of the minimum drag coefficient for each of the wing positions at each Mach number have been included to give an indication of the magnitude of the uncertainty in the measurement of drag coefficient. These data indicate the average minimum drag with the wing in the high position to have been slightly lower than with the wing in the mid position. However, the lift-drag ratio with the wing in the high position was, in general, slightly lower than for the wing in the mid position. (See fig. 23.) This latter result is in agreement with the results reported in reference 9.

The values of lift-drag ratio measured during the tests reported in reference 9 for a wing of the same plan form, but with a thickness-chord ratio of 3 percent, were greater by between 10 and 20 percent than those obtained during the present investigation. The higher minimum drags measured during the present investigation due to the presence of a vertical tail account for part of this difference. The remainder of the difference in lift-drag ratio was caused by a higher drag due to lift. The difference in drag due to lift might be due to a difference in Reynolds number, the Reynolds numbers being 2.5 million for the present tests and 3.1 and 4.8 million for the tests reported in reference 9.

Effects of tail size and location. The preceding discussion has illustrated that the drag data from this investigation should be used with caution if comparisons are to be made with results of tests of other configurations at different Reynolds numbers. For this reason, the difference in lift-drag ratio between the tail-off and the balanced,

tail-on conditions is presented rather than the total lift-drag ratio for the balanced condition. These data, which were taken from faired curves, are presented in figure 24. In general, the drag increment due to balancing the model decreased with increases in tail size or length, was less for the lower tail position, and increased rapidly as the Mach number was increased beyond 0.90. These trends can be easily verified by estimating the increment in lift-drag ratio due to balancing the model from the tail-off pitching-moment coefficients and the increase in minimum drag coefficient caused by the tail. Such an estimation has been made wherein it was assumed that the lift contribution of the tail was equivalent to the force on the tail normal to the fuselage center line, and that the induced drag caused by this lift was equivalent to that for an elliptical span-load distribution. The following equations for the drag polar for the balanced condition resulted:

$$\begin{array}{l} {^{C}L_{C_{m}}}=0 \end{array} = {^{C}L_{tail}} \hspace{0.1cm} \text{off} \hspace{0.1cm} + \hspace{0.1cm} \frac{{^{C_{m}}}{tail} \hspace{0.1cm} \text{off}}{\imath_{t}/\bar{c}} \\ \\ {^{C}D_{C_{m}}}=0 \end{array} = {^{C}D_{tail}} \hspace{0.1cm} \text{off} \hspace{0.1cm} + \hspace{0.1cm} \Delta^{C_{D_{O}}} \hspace{0.1cm} \text{otail} \hspace{0.1cm} + \hspace{0.1cm} \left(\frac{S_{t}}{S_{w}}\right) \frac{\left(\frac{C_{m_{tail}} \hspace{0.1cm} \text{off}}{V_{h}}\right)^{2}}{\pi A_{tail}} \end{array}$$

The value of  $\Delta^{C}_{Dotail}$  was taken as the average measured increment in drag at zero lift caused by the tail at an incidence of 0.2°. The following table lists these values:

	${ m \Delta c_{Do}}_{ m tail}$			
M	St = 0.167 Sw	$S_t = 0.219 S_w$		
0.60 .80 .90 .95	0.0009 .0009 .0010 .0020	0.0012 .0012 .0014 .0028		

The increment in lift-drag ratio due to balancing the model, evaluated by this method, is presented in figure 25. The calculated increment is, in general, slightly greater than that obtained from the drag measurements, but the effects of tail size, tail length, tail height, and Mach number are in qualitative agreement with those obtained directly from the drag measurements.

A large part of the effect of tail size and position on the lift-drag ratio for the balanced condition at a given lift coefficient was dependent upon the magnitude and the algebraic sign of the tail lift. This accounts for the smaller decrement of lift-drag ratio for the larger tail volumes and for the lower tail position. The large decrease in the lift-drag ratio due to balancing the model at Mach numbers greater than 0.90 was a result of a decreasing load on the horizontal tail (or increasing down load) with increasing Mach number as well as the large increase in the minimum drag increment due to the tail,

#### CONCLUDING REMARKS

The present wind-tunnel investigation has evaluated the effects of tail position and size on the aerodynamic characteristics of an airplane configuration having a thin triangular wing of aspect ratio 3. It was found that the horizontal tail was destabilizing at moderate lift coefficients when placed either 10 or 20 percent of the wing semispan above the wing chord plane, and stabilizing throughout the lift range when placed either in the wing chord plane or 10 percent of the wing semispan below this plane. For the latter locations of the horizontal tail, the drag due to balancing the model was found to decrease with increases in either tail size or tail length, was less with the tail below the wing chord plane, and increased markedly with increases in Mach numbers beyond 0.90.

Ames Aeronautical Laboratory
National Advisory Committee for Aeronautics
Moffett Field, Calif., Dec. 15, 1953

#### REFERENCES

- 1. Savage, Howard F., and Tinling, Bruce E.: The Subsonic Static Aerodynamic Characteristics of an Airplane Model Having a Triangular Wing of Aspect Ratio 3. II Lateral and Directional Characteristics. NACA TN 4042, 1957. (Supersedes NACA RM A55Bll.)
- 2. Tinling, Bruce E., and Karpen, A. V.: The Subsonic Static Aerodynamic Characteristics of an Airplane Model Having a Triangular Wing of Aspect Ratio 3. III Effects of Trailing-Edge Flaps. NACA TN 4043, 1957. (Supersedes NACA RM A54L07.)
- 3. Buell, Donald A., and Tinling, Bruce E.: Ground Effects on The Longitudinal Characteristics of Two Models with Wings Having Low Aspect Ratio and Pointed Tips. NACA TN 4044, 1957. (Supersedes NACA RM A55E04.)

- 4. Koenig, David G.: Tests in the Ames 40- by 80-Foot Wind Tunnel of an Airplane Configuration With an Aspect Ratio 3 Triangular Wing and an All-Movable Horizontal Tail Longitudinal and Lateral Characteristics. NACA RM A52Ll5, 1953.
- 5. Axelson, John A.: Downwash Behind a Triangular Wing of Aspect Ratio 3 Transonic Bump Method. NACA RM A53123, 1953.
- 6. DeYoung, John, and Harper, Charles W.: Theoretical Symmetric Span Loading at Subsonic Speeds for Wings Having Arbitrary Plan Form. NACA Rep. 921, 1950.
- 7. Sivells, James C., and Salmi, Rachel M.: Jet-Boundary Corrections for Complete and Semispan Swept Wings in Closed Circular Wind Tunnels. NACA TN 2454, 1951.
- 8. Herriot, John G.: Blockage Corrections for Three-Dimensional-Flow Closed-Throat Wind Tunnels, With Consideration of the Effect of Compressibility. NACA Rep. 995, 1950. (Supersedes NACA RM A7B28.)
- 9. Heitmeyer, John C.: Effect of Vertical Position of the Wing on the Aerodynamic Characteristics of Three Wing-Body Combinations. NACA RM A52L15a, 1953.

## TABLE I.- GEOMETRIC PROPERTIES OF THE MODEL

Wing				
Aspect ratio				
Aspect ratio				
Large tail				
Large tail				
Vertical tail (leading and trailing edges extended to fuselage center line)				
Aspect ratio (geometric)				
Fuselage				
Fineness ratio Short fuselage				

TABLE I. - GEOMETRIC PROPERTIES OF THE MODEL - Concluded

Fuselage - continued			
Base area Coordinates (long	fuselage):		0.1302 ft <sup>2</sup>
	Distance from nose, inches	Radius, inches	
	0 5.00 10.00 15.00 20.00 25.00 30.00 35.00 40.00 45.00 51.25 57.75 61.75 69.75 72.00	0 .80 1.44 1.94 2.32 2.60 2.79 2.90 2.97 2.99 3.00 3.00 2.99 2.99 2.67 2.44	

<sup>&</sup>lt;sup>1</sup>Removable section from 51.25 to 57.75 inches from nose

TABLE II.- MOMENT CENTERS, TAIL LENGTHS, AND TAIL VOLUMES

Tail height, z/(b/2)	Tail size, $S_{\rm t}/S_{\rm w}$	Moment center	Tail length, $l_t/\bar{c}$	Tail volume, $V_{ m h}$
-0.10 .10 .10 .20 .20	0.167 .167 .219 .219 .167 .167 .219 .167 .219 .167	0.342ē .365ē .372ē .415ē .330ē .349ē .346ē .375ē .381ē .379ē .405ē	1.183 1.510 1.153 1.460 1.195 1.526 1.179 1.500 1.494 1.146 1.470	0.198 .252 .253 .320 .199 .254 .258 .328 .249 .251 .246

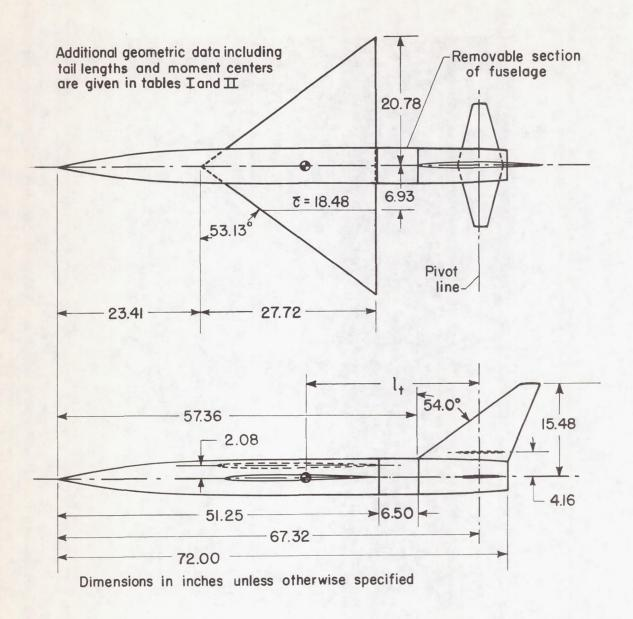
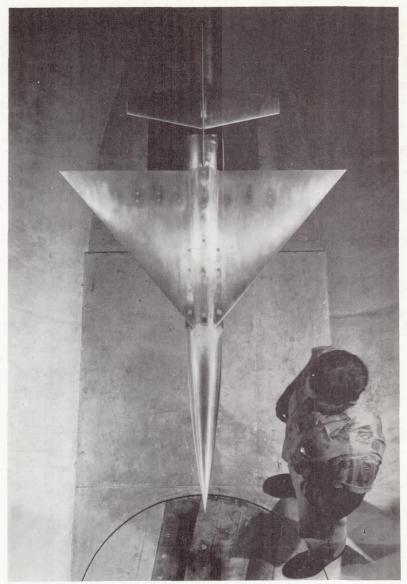


Figure 1.- Geometry of the model.



A -18664

Figure 2.- Model mounted in the wind tunnel.

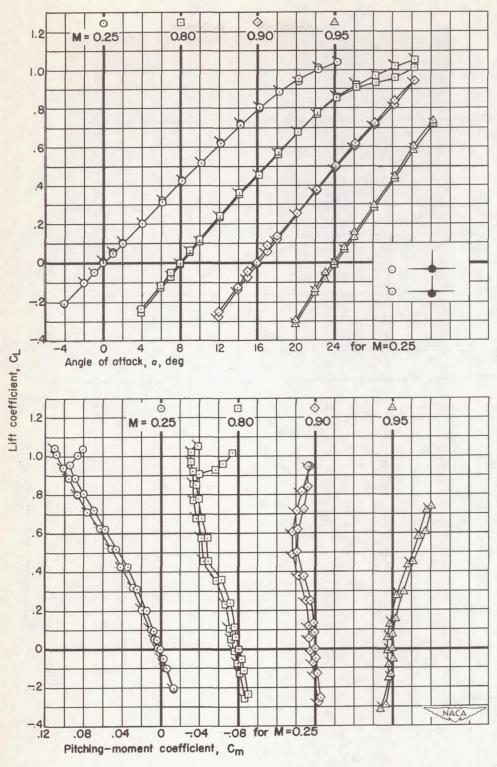


Figure 3.- The tail-off lift and pitching-moment characteristics for the mid and high positions of the wing. Moment center, 0.415c.

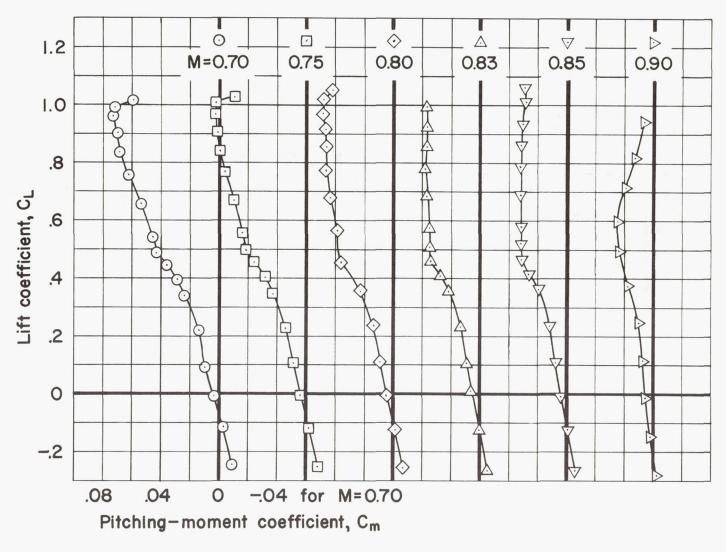
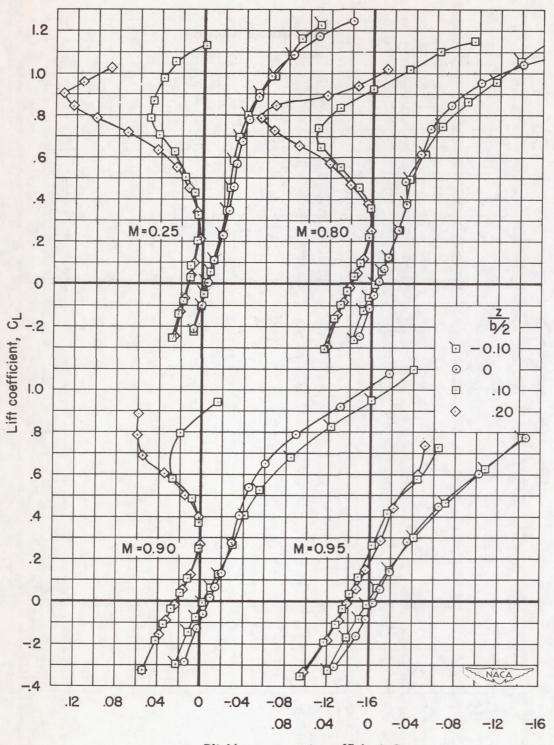


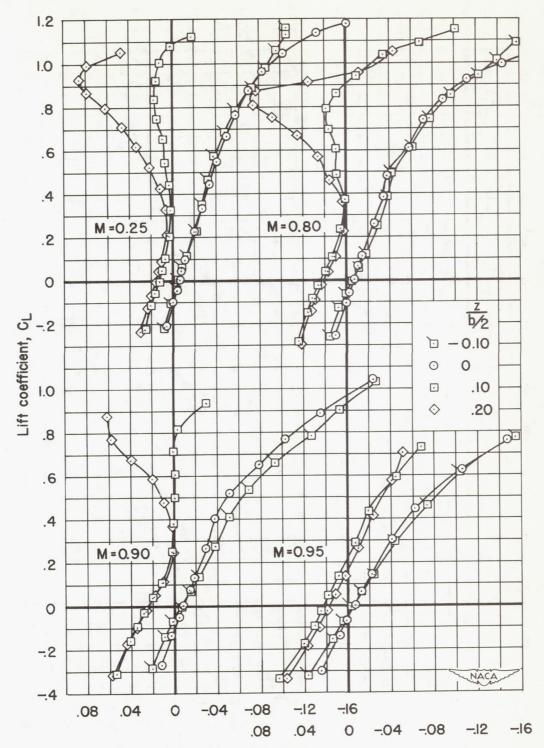
Figure 4.- The tail-off pitching-moment characteristics with the wing in the high position for Mach numbers from 0.70 to 0.90. Moment center, 0.415c.



Pitching-moment coefficient, C<sub>m</sub>

(a)  $l_t/\bar{c} \approx 1.2$ ,  $S_t/S_W = 0.219$ 

Figure 5.- The effect of tail height on the pitching-moment characteristics.  $i_t = 0^{\circ}$ .



Pitching-moment coefficient, C<sub>m</sub>

(b)  $l_t/\bar{c} \approx 1.5$ ,  $S_t/S_w = 0.167$ 

Figure 5. - Concluded.

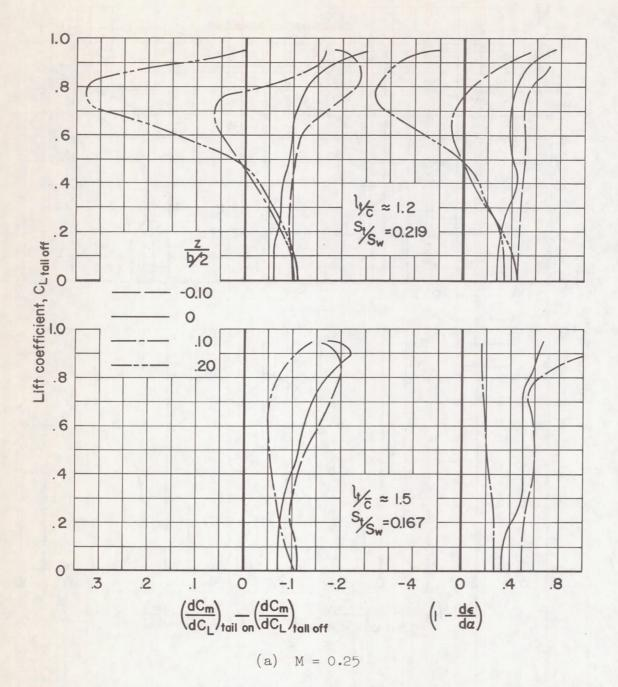
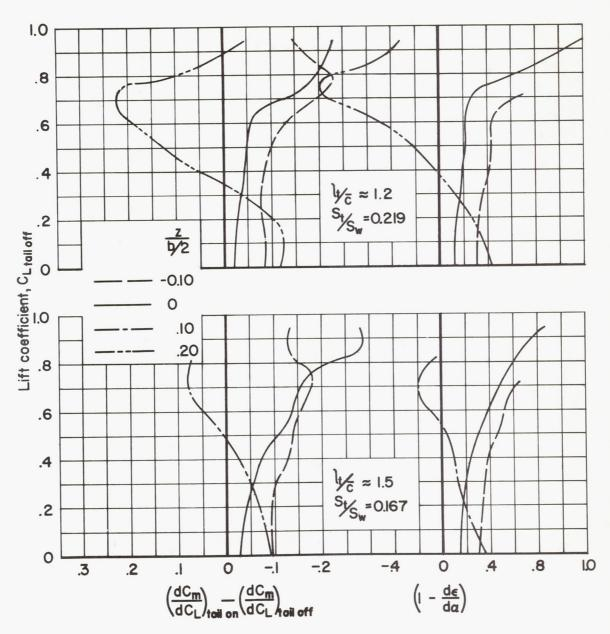


Figure 6.- The variations with lift coefficient of the contribution of the horizontal tail to the longitudinal stability and the downwash factor  $\left(1-\frac{d\varepsilon}{d\alpha}\right)$ .  $i_t\approx 0$ .



(b) M = 0.90

Figure 6.- Concluded.

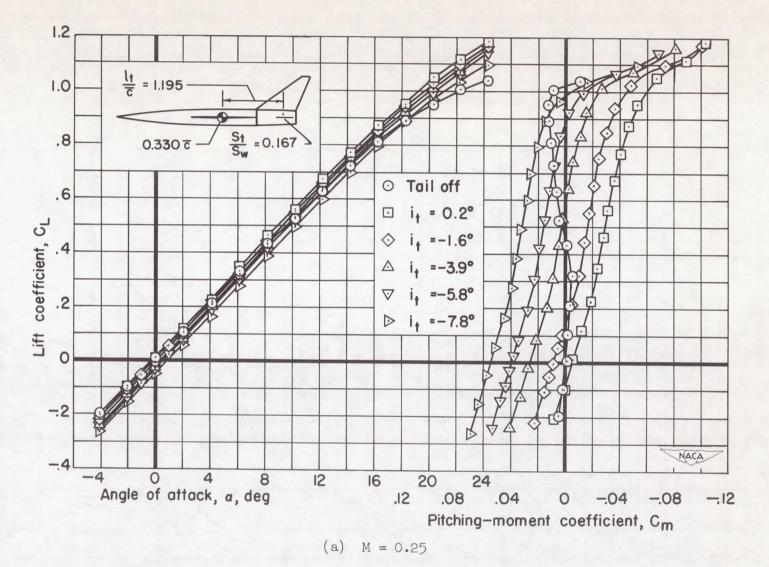


Figure 7.- Lift and pitching-moment characteristics. Moment center at 0.330 $\bar{c}$ ,  $l_t/\bar{c}$  = 1.195,  $s_t/s_w$  = 0.167,  $\frac{z}{b/2}$  = 0.

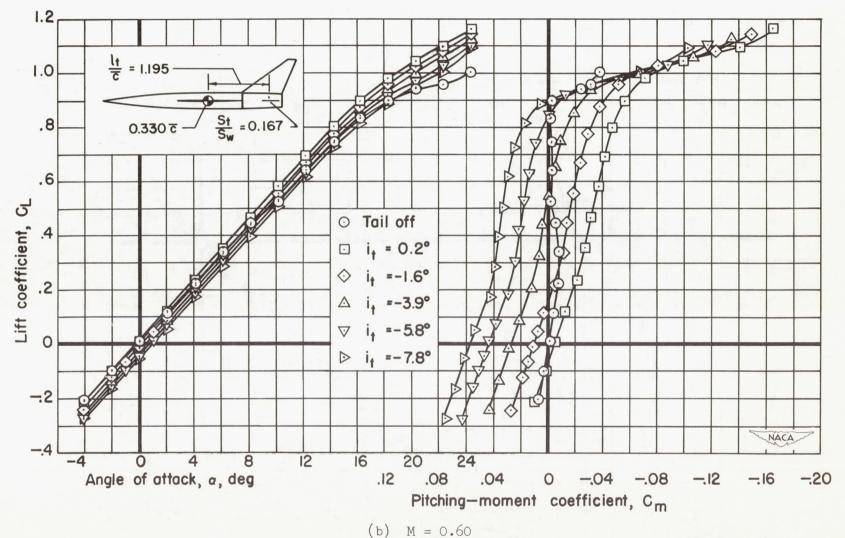


Figure 7.- Continued.

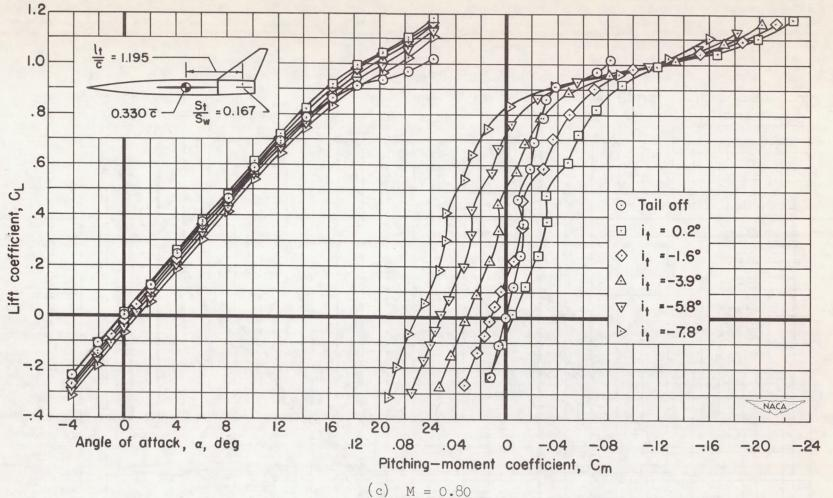


Figure 7. - Continued.

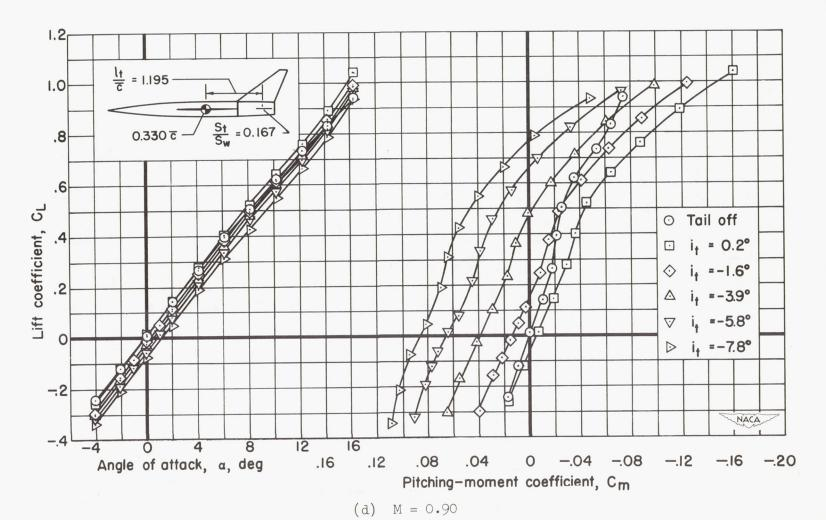


Figure 7 .- Continued.

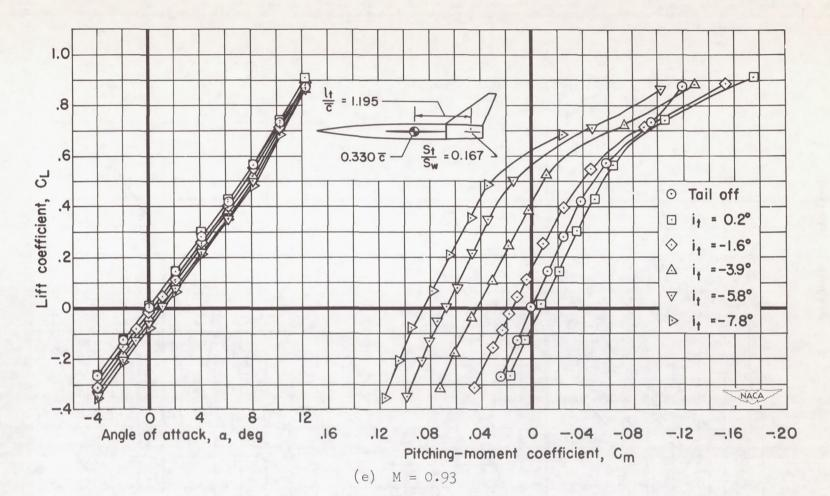
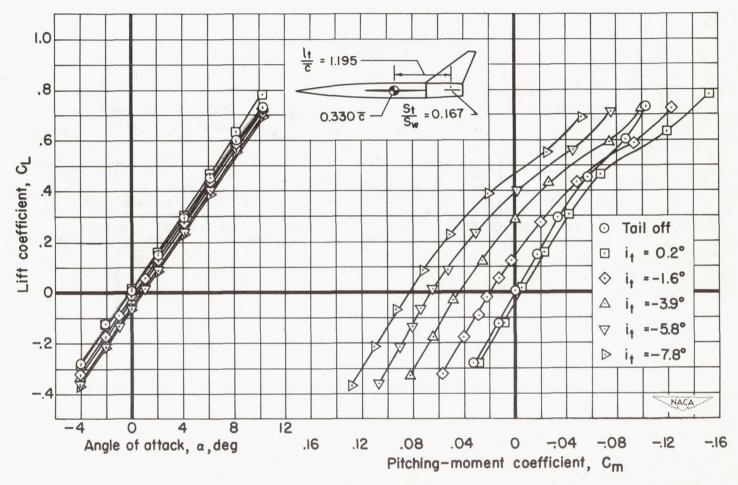


Figure 7.- Continued.



(f) M = 0.95

Figure 7.- Concluded.

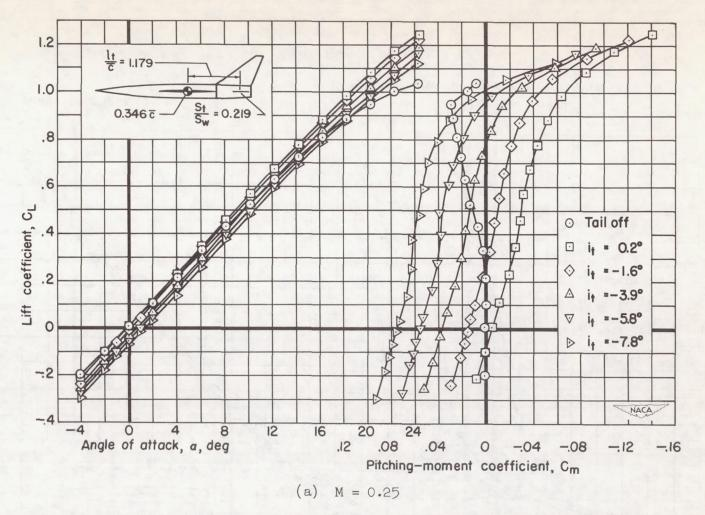
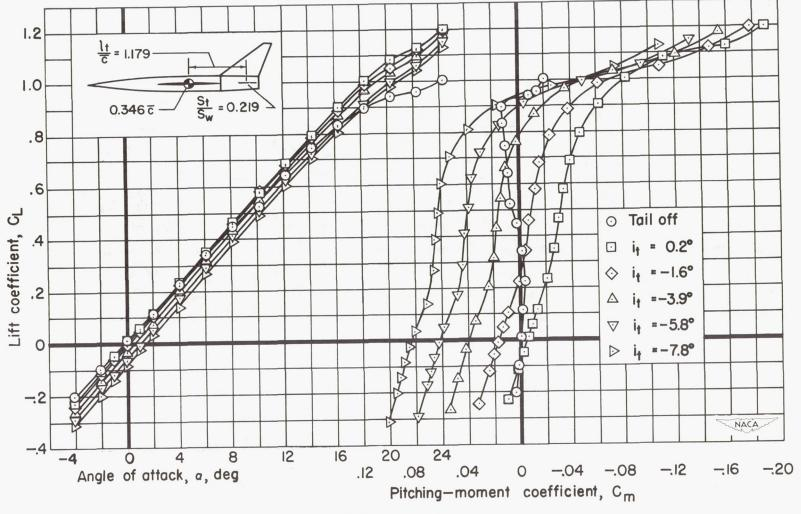


Figure 8.- Lift and pitching-moment characteristics. Moment center at 0.346 $\bar{c}$ ,  $l_t/\bar{c}$  = 1.179,  $S_t/S_W$  = 0.219,  $\frac{z}{b/2}$  = 0.



(b) M = 0.60

Figure 8.- Continued.

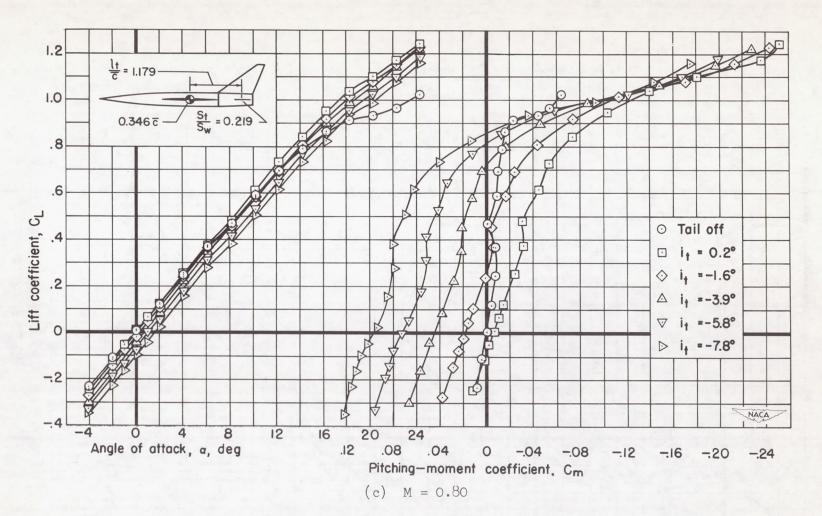
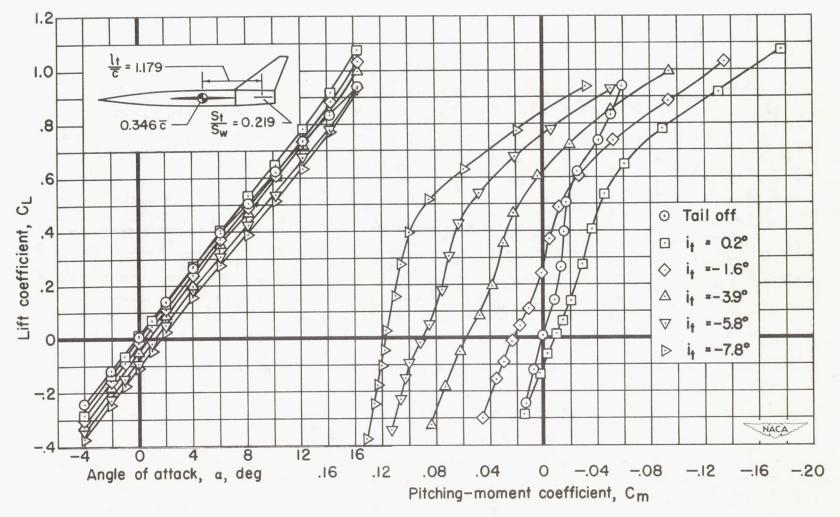


Figure 8.- Continued.



(d) M = 0.90

Figure 8.- Continued.

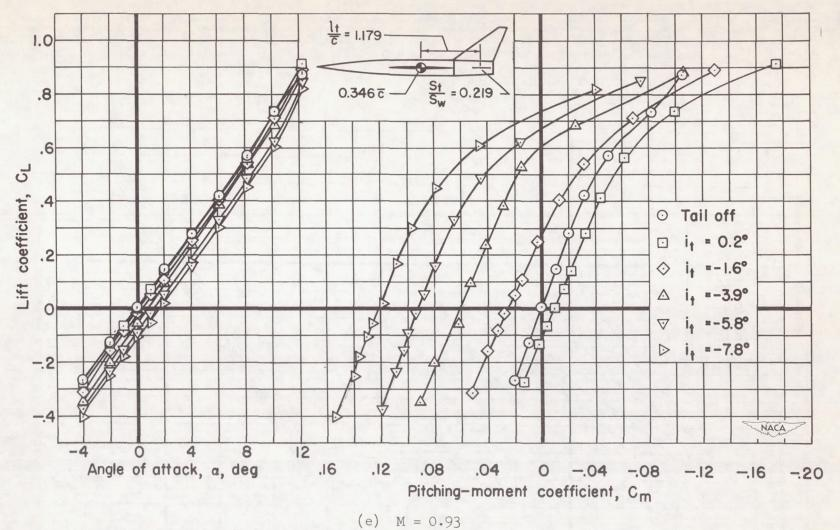


Figure 8. - Continued.

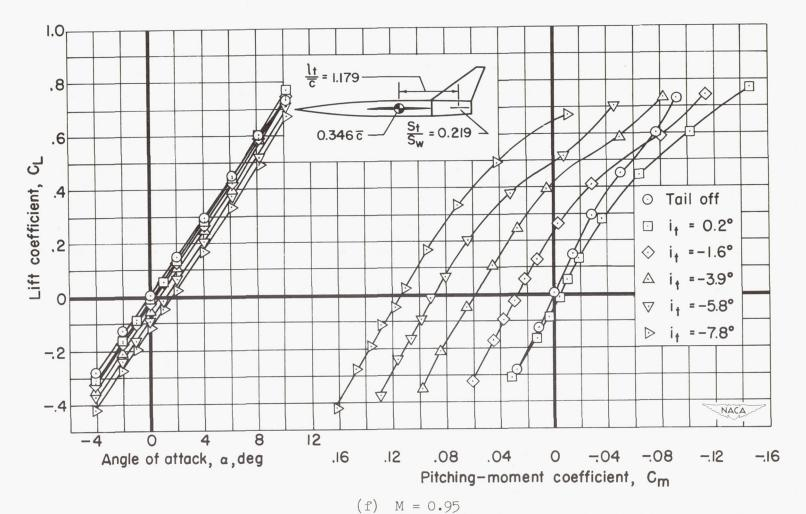


Figure 8.- Concluded.

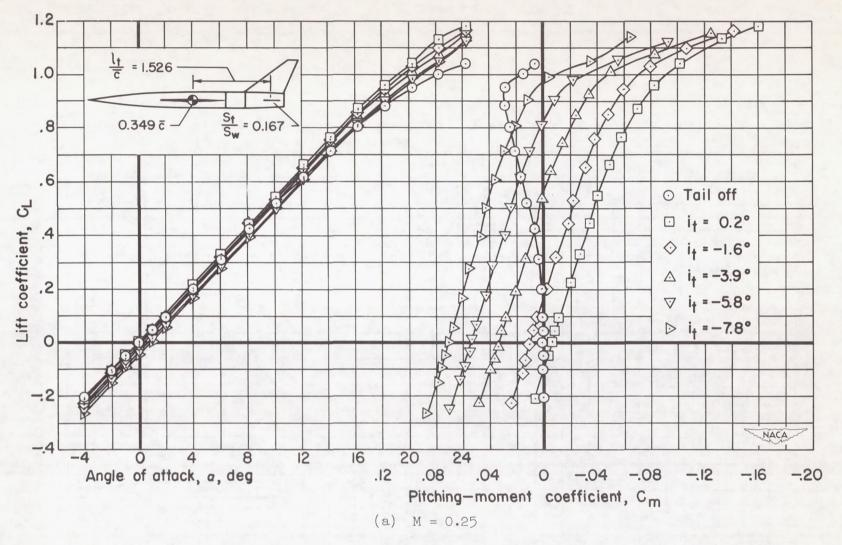


Figure 9.- Lift and pitching-moment characteristics. Moment center at 0.349 $\bar{c}$ ,  $l_t/\bar{c}$  = 1.526,  $s_t/s_w$  = 0.167,  $\frac{z}{b/2}$  = 0.

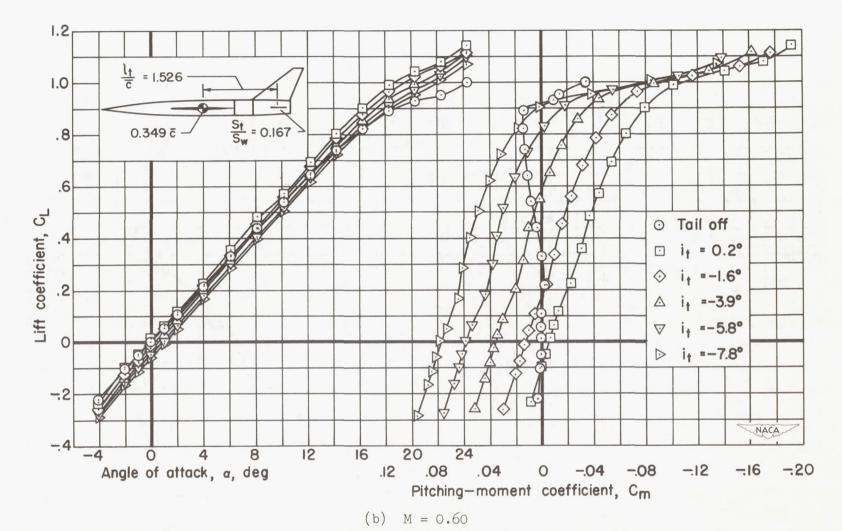
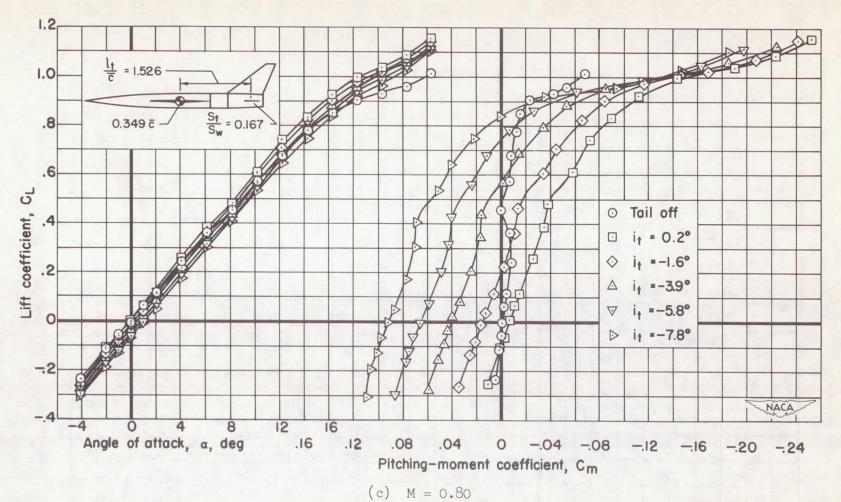
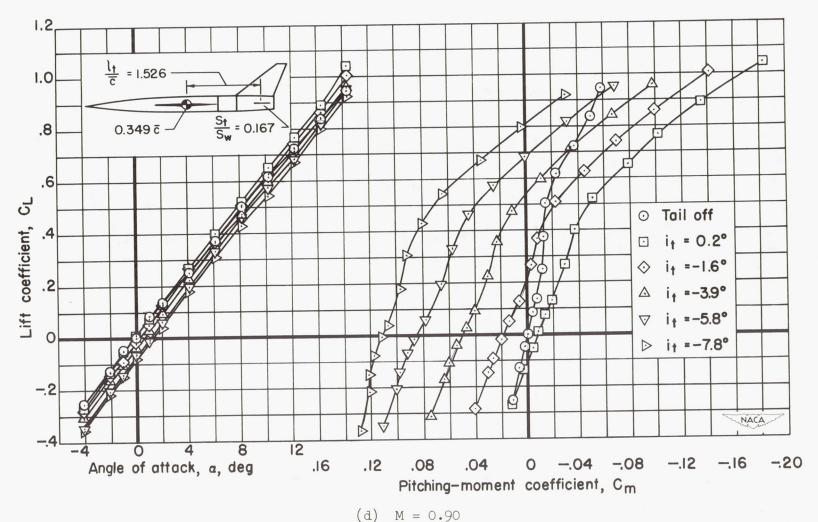


Figure 9.- Continued.



(c) M = 0.00

Figure 9.- Continued.



(d) M = 0.90

Figure 9. - Continued.

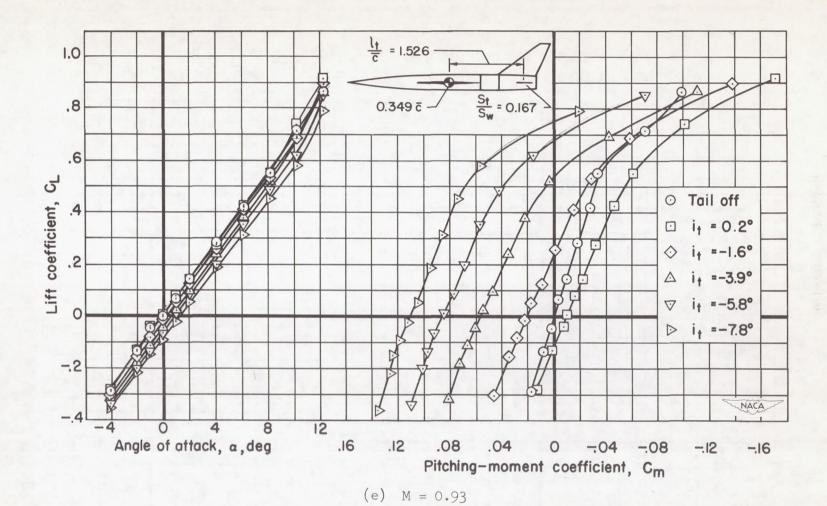


Figure 9.- Continued.

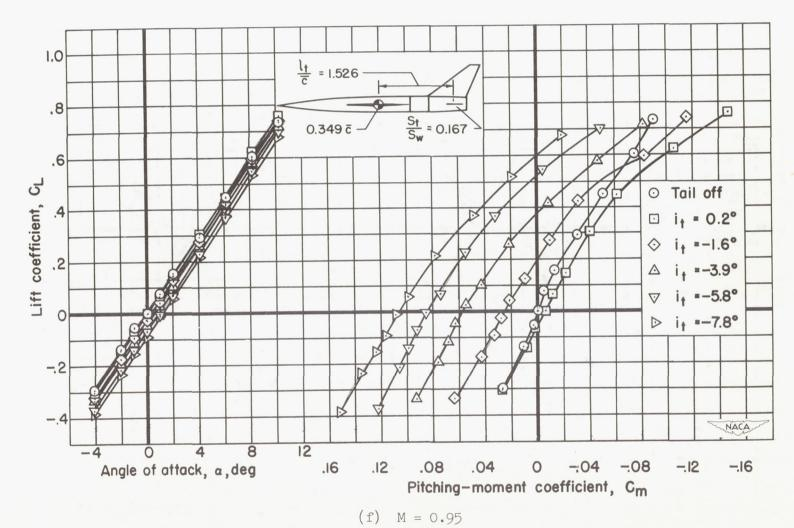


Figure 9.- Concluded.

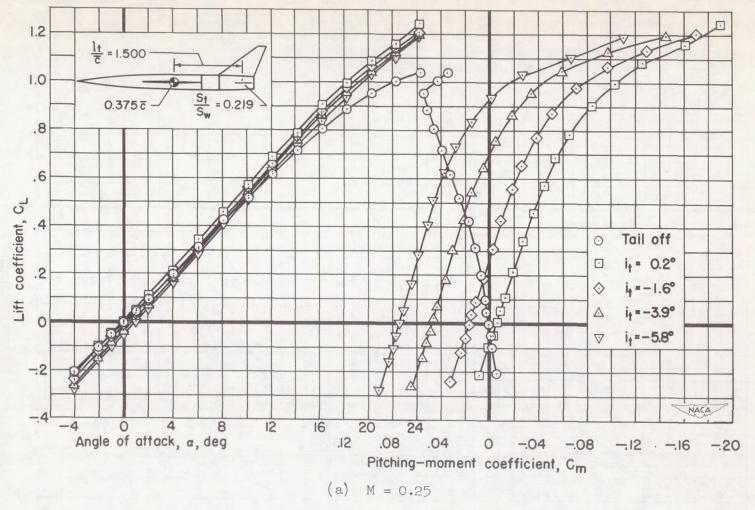


Figure 10.- Lift and pitching-moment characteristics. Moment center at 0.375 $\bar{c}$ ,  $l_t/\bar{c}$  = 1.500,  $S_t/S_w$  = 0.219,  $\frac{z}{b/2}$  = 0.

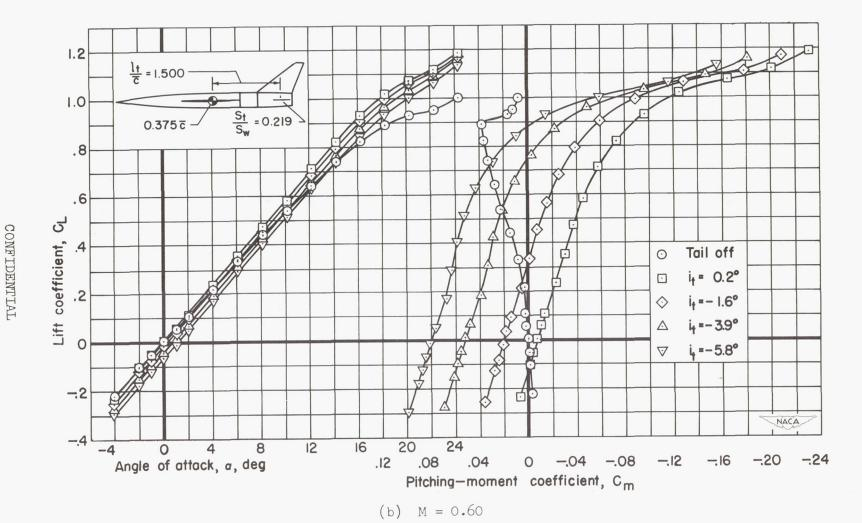


Figure 10. - Continued.

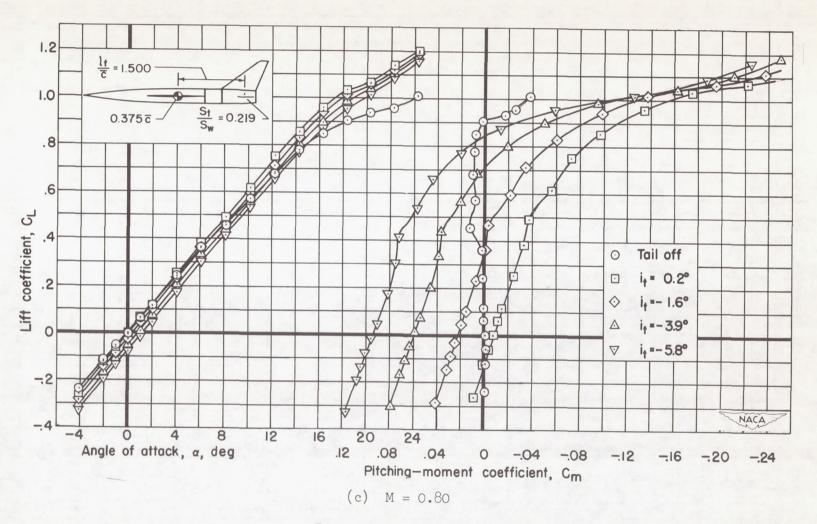
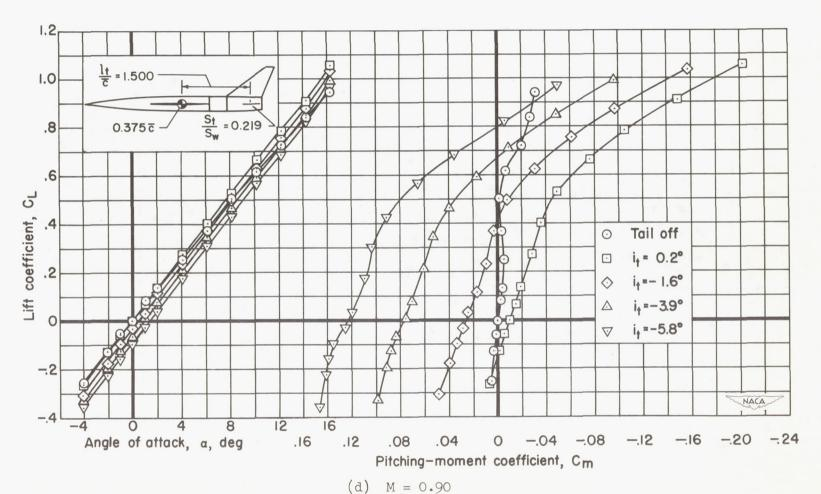
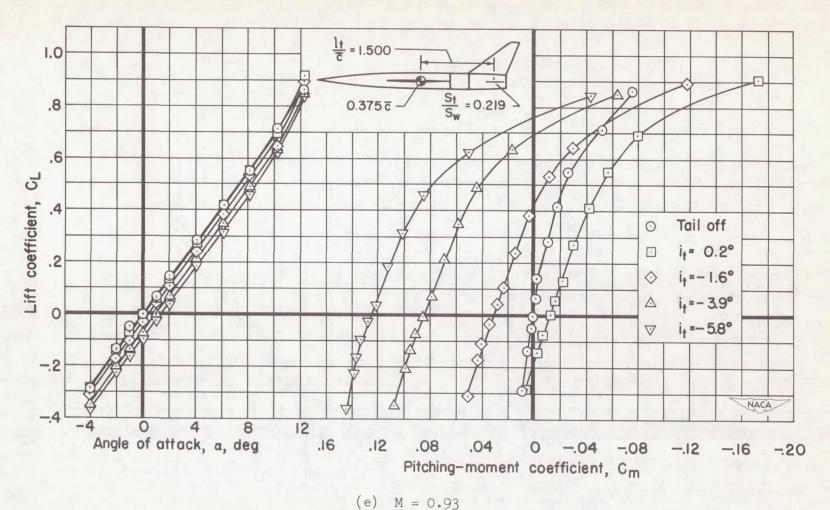


Figure 10. - Continued.



(--/

Figure 10. - Continued.



(0) 11 - 0.93

Figure 10. - Continued.

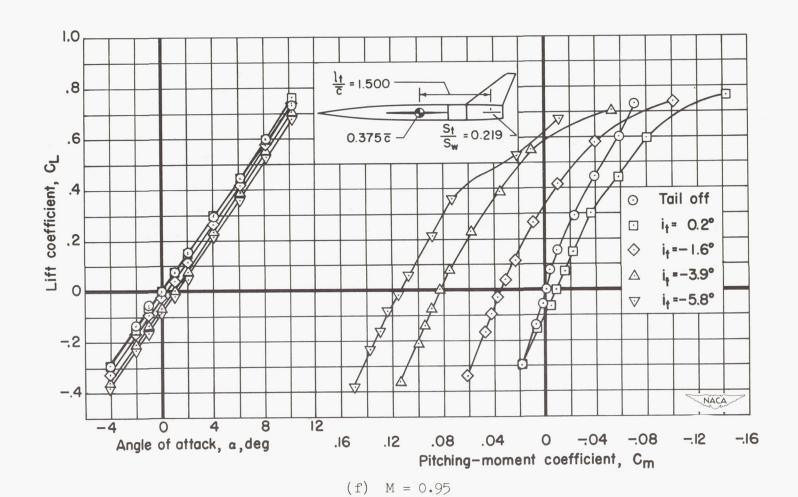


Figure 10.- Concluded.

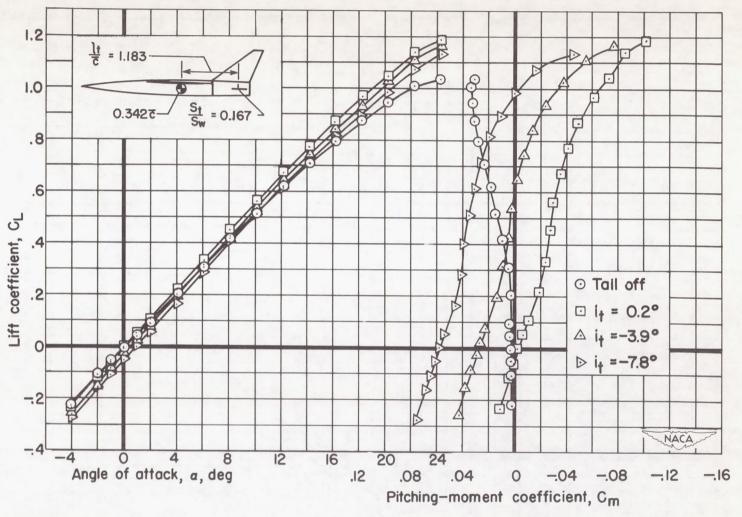
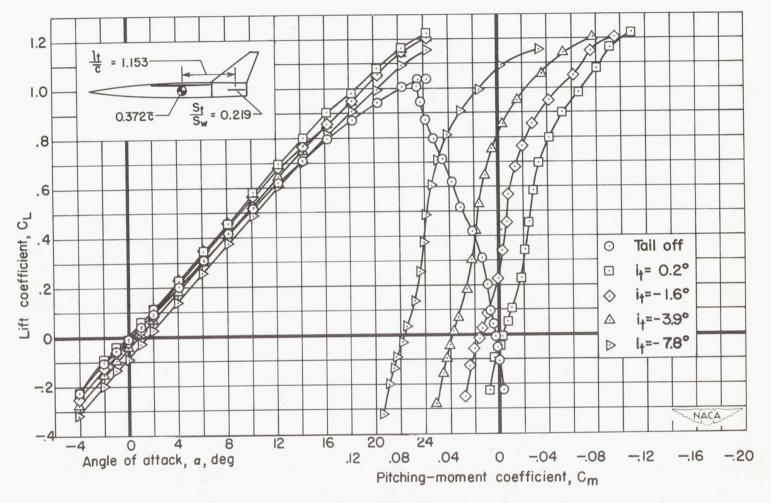


Figure 11.- Lift and pitching-moment characteristics. M = 0.25, moment center at 0.342 $\bar{c}$ ,  $l_t/\bar{c}$  = 1.183,  $S_t/S_W$  = 0.167,  $\frac{z}{b/2}$  = -0.10.



(a) M = 0.25

Figure 12.- Lift and pitching-moment characteristics. Moment center at 0.372 $\bar{c}$ ,  $l_t/\bar{c}$  = 1.153,  $s_t/s_w$  = 0.219,  $\frac{z}{b/2}$  = -0.10.

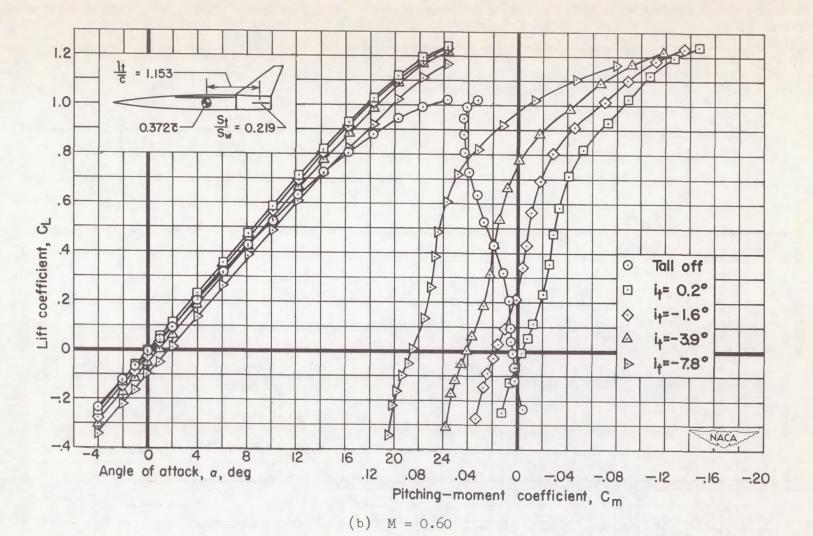
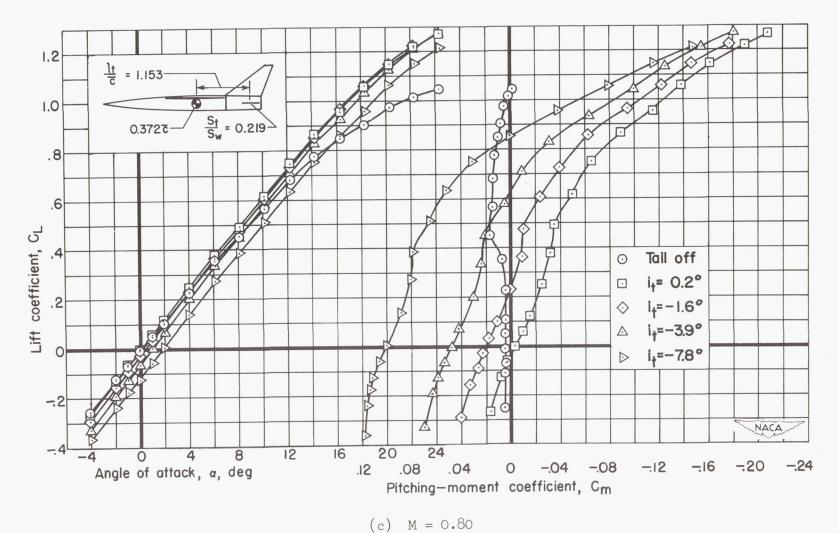
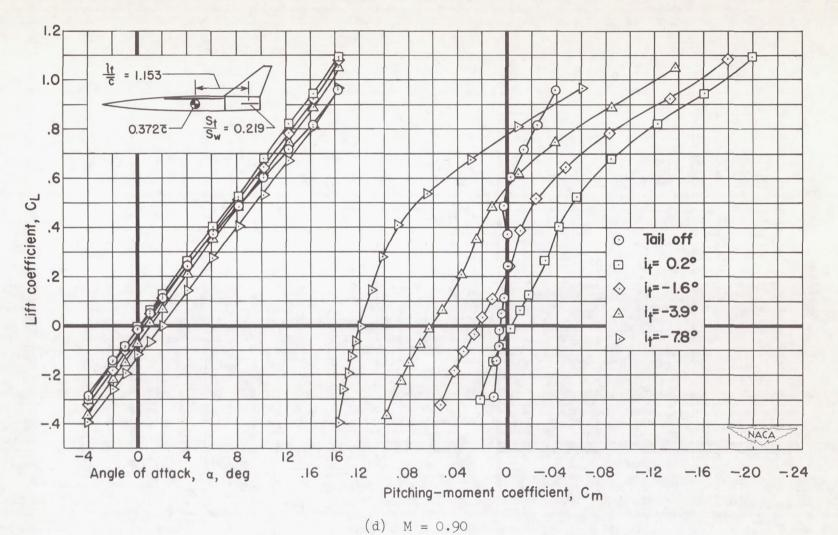


Figure 12. - Continued.



(c) 11 = 0.00

Figure 12. - Continued.



(4)

Figure 12.- Continued.

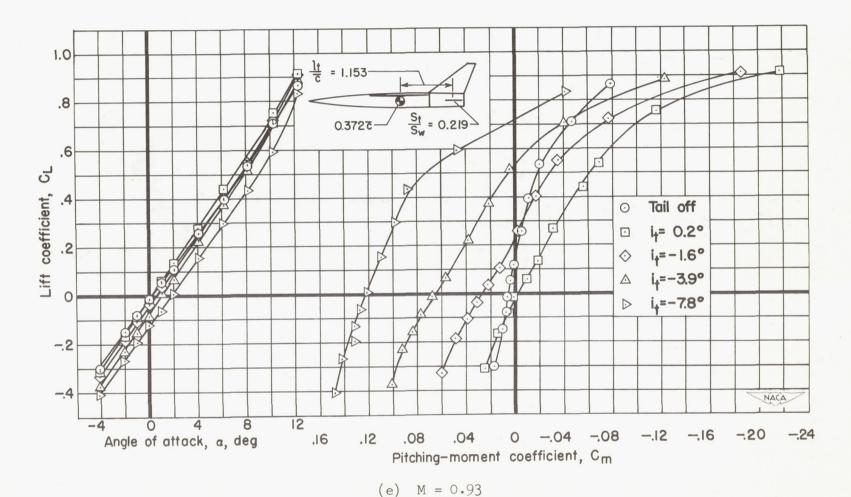


Figure 12. - Continued.

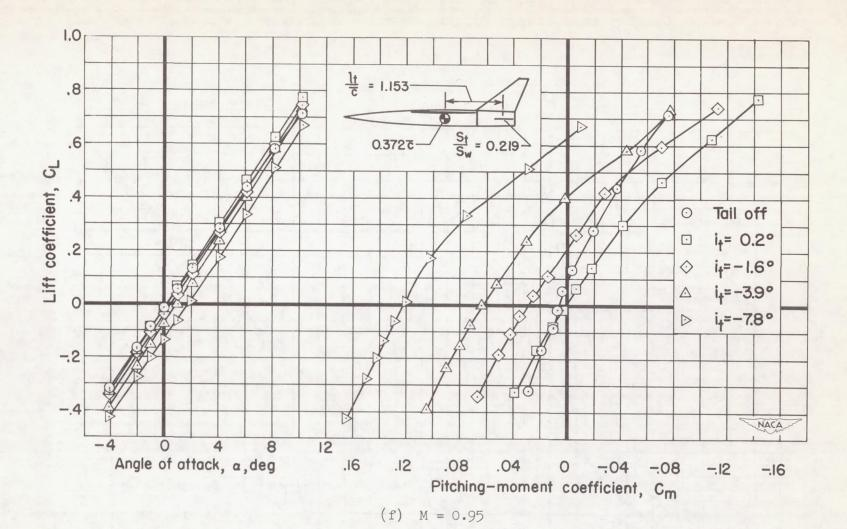


Figure 12.- Concluded.

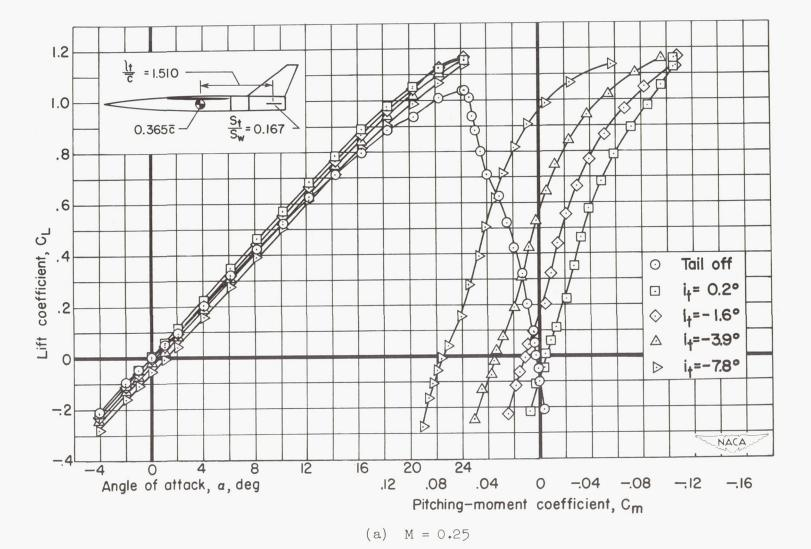
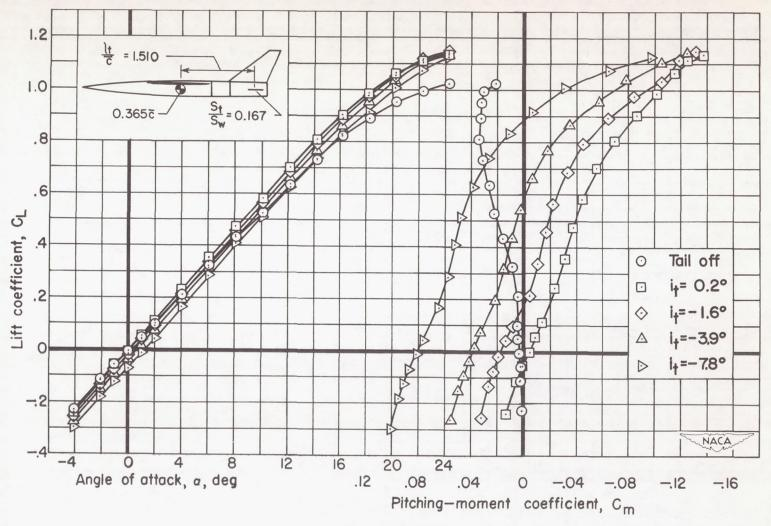


Figure 13.- Lift and pitching-moment characteristics. Moment center at 0.365 $\bar{c}$ ,  $l_t/\bar{c}$  = 1.510,  $S_t/S_w$  = 0.167,  $\frac{z}{b/2}$  = -0.10.



(b) M = 0.60

Figure 13.- Continued.

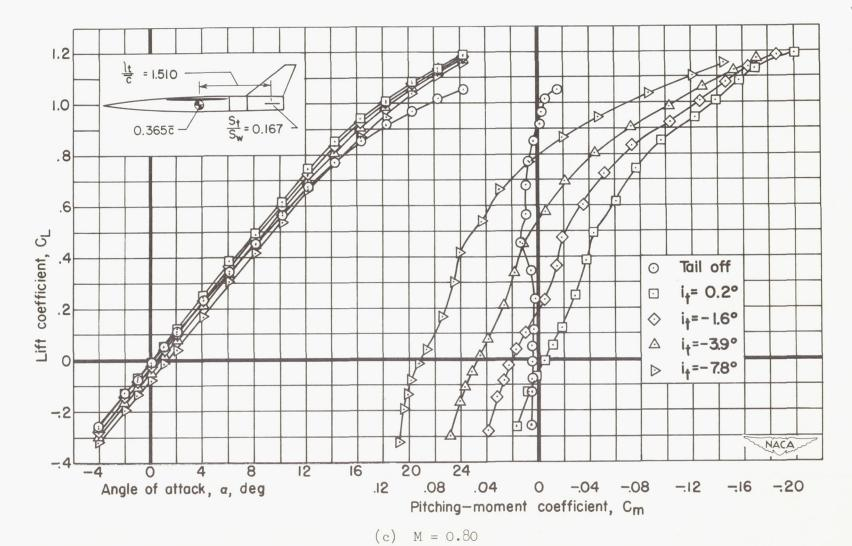
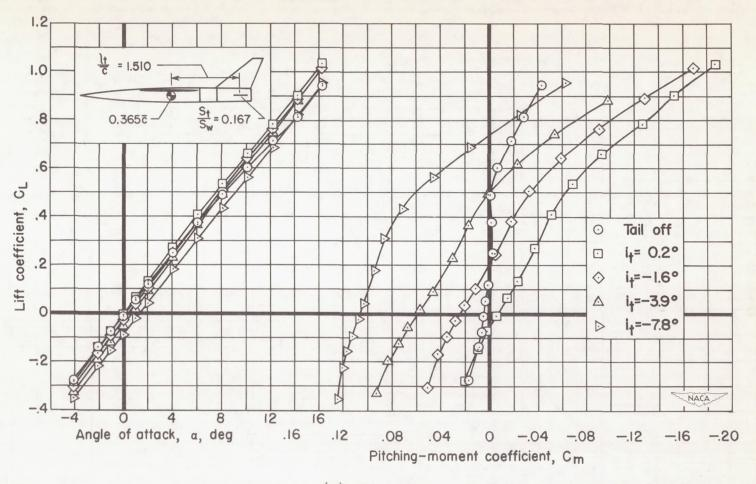


Figure 13. - Continued.



(d) M = 0.90

Figure 13. - Continued.

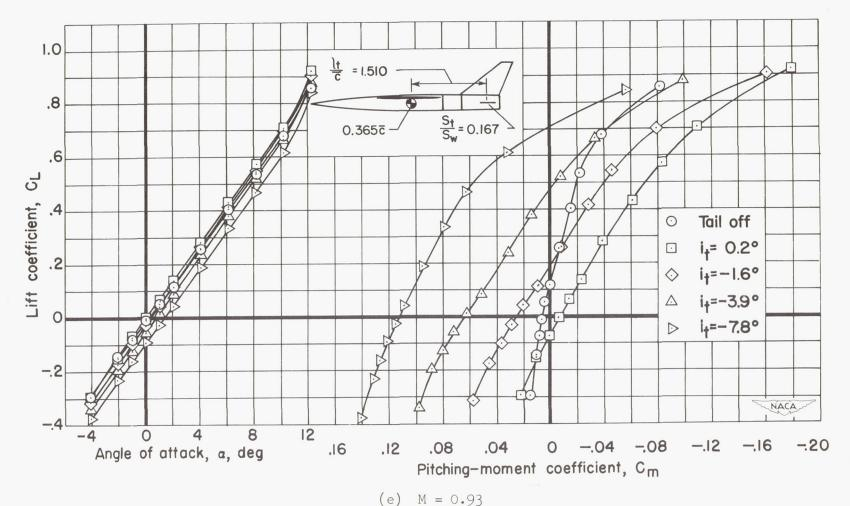


Figure 13.- Continued.

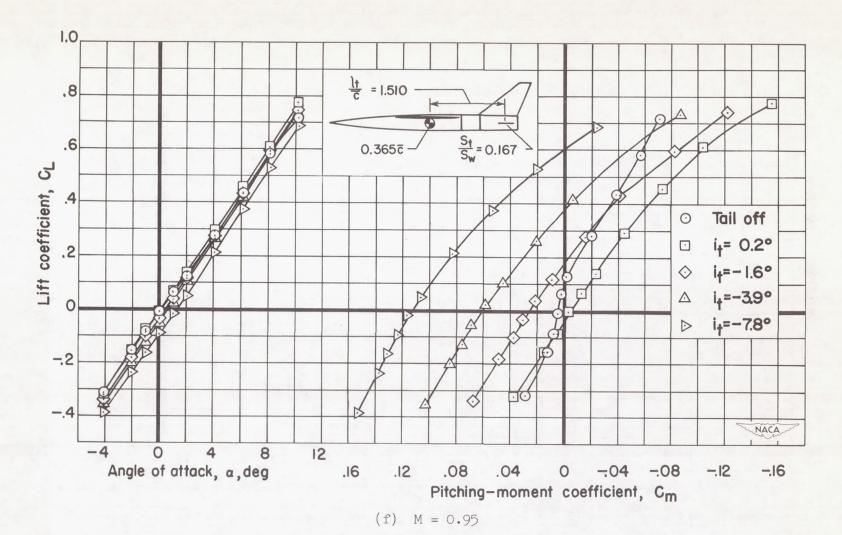


Figure 13.- Concluded.

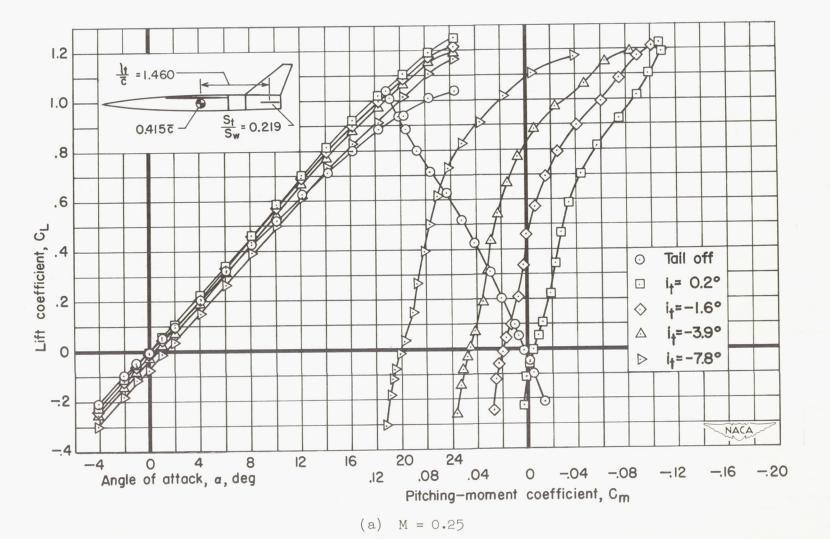


Figure 14.- Lift and pitching-moment characteristics. Moment center at 0.415 $\bar{c}$ ,  $l_t/\bar{c}$  = 1.460,  $S_t/S_w$  = 0.219,  $\frac{z}{b/2}$  = -0.10.

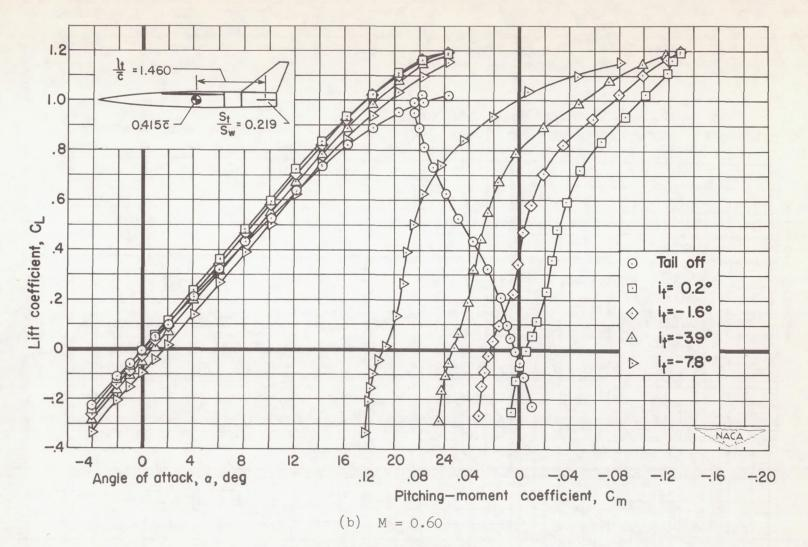
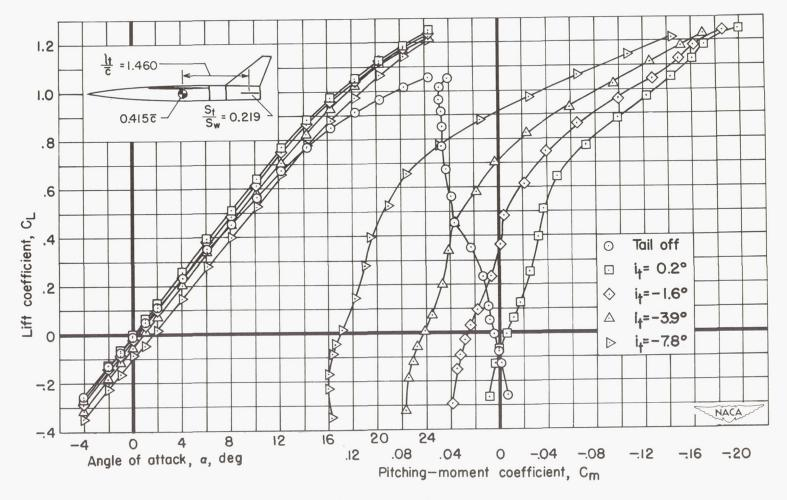


Figure 14. - Continued.



(c) M = 0.80

Figure 14. - Continued.

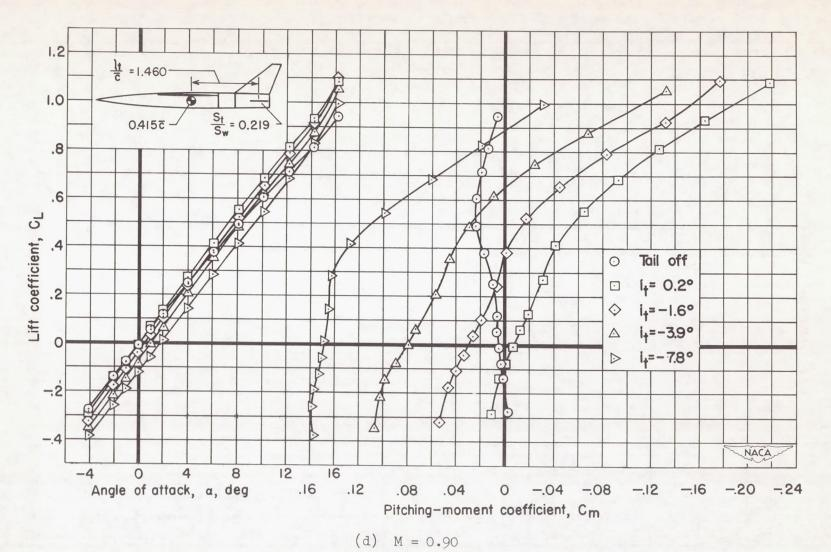


Figure 14.- Continued.

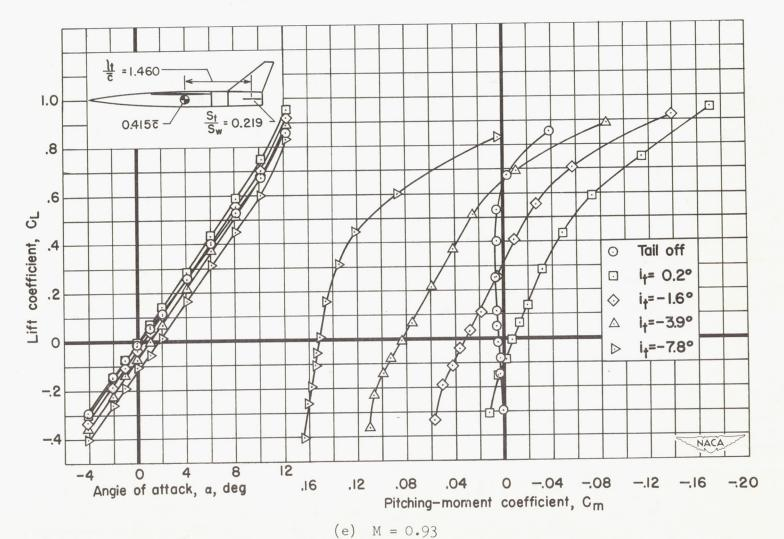


Figure 14. - Continued.

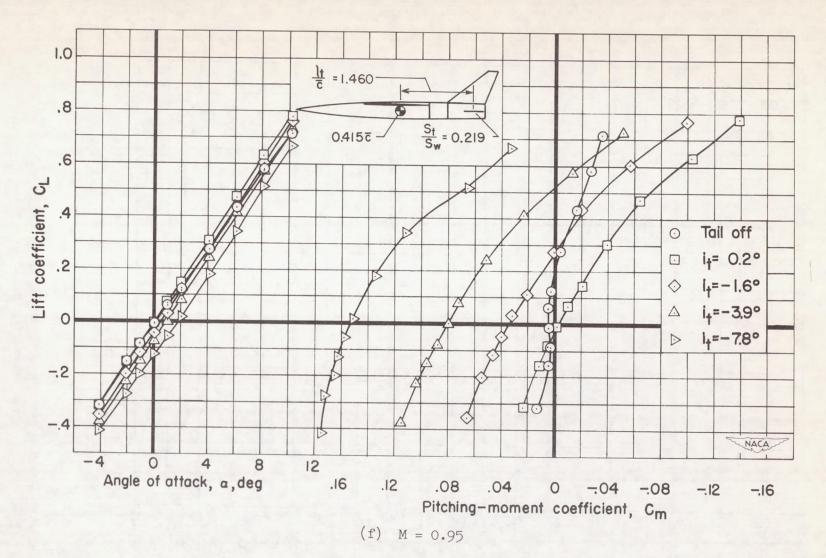


Figure 14. - Concluded.

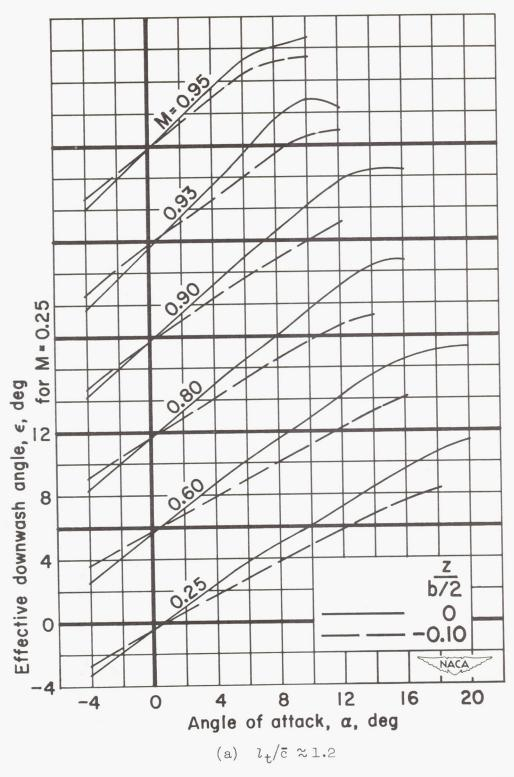


Figure 15.- The variation with angle of attack of the average effective downwash for both tail sizes.

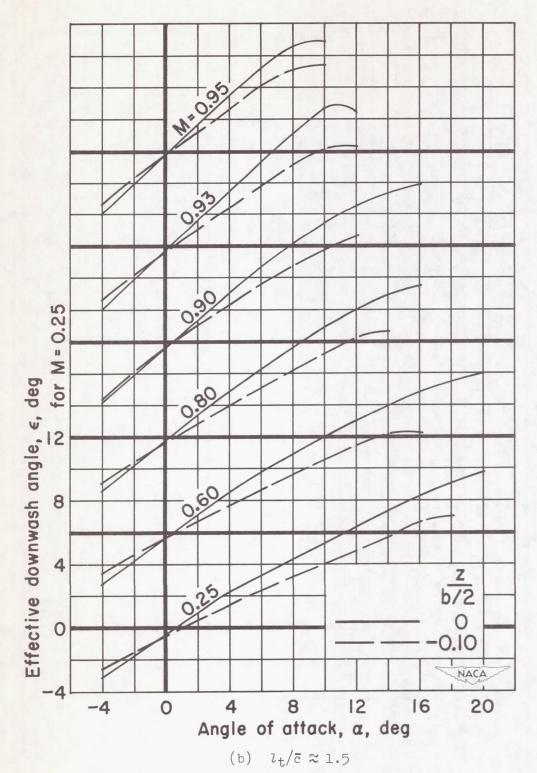


Figure 15.- Concluded.

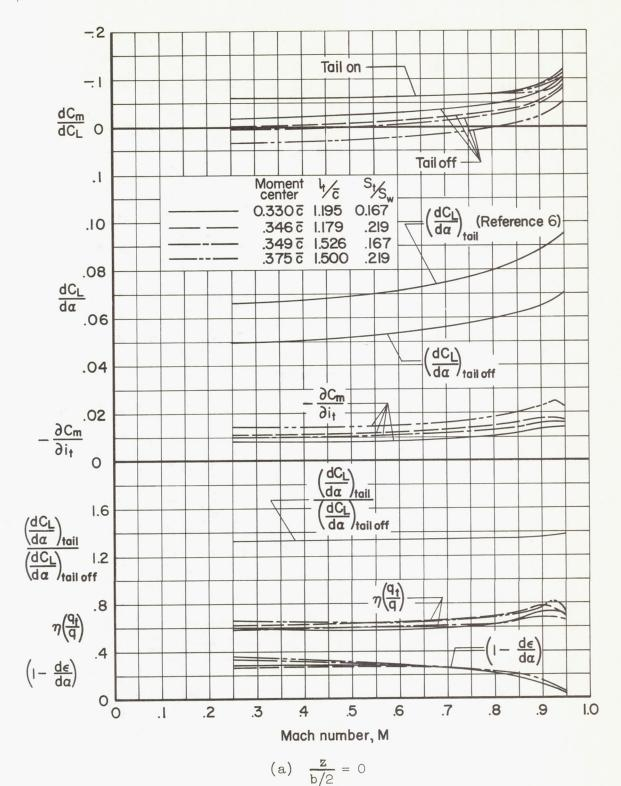


Figure 16.- The variation with Mach number of the tail control effectiveness, the static longitudinal stability, and the factors contributing to the static longitudinal stability.  $C_{\rm L}$  = 0.

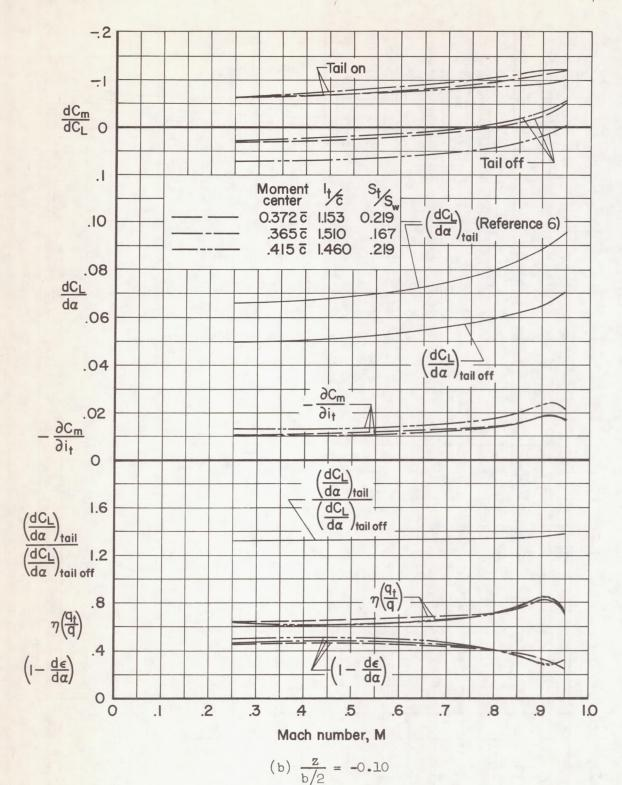


Figure 16.- Concluded.

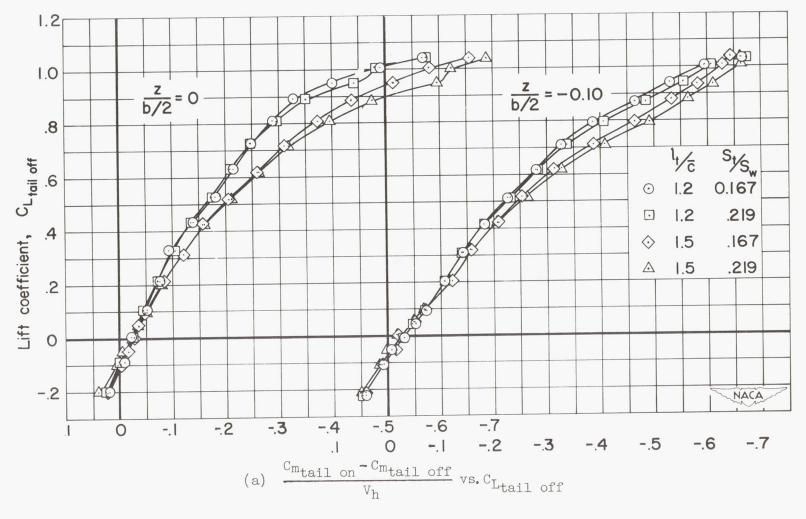


Figure 17.- The variations of the pitching-moment coefficient due to the horizontal tail and of the factors  $\frac{(dC_L/d\alpha)_{tail}}{(dC_L/d\alpha)_{tail}}$  and  $\left(1-\frac{d\varepsilon}{d\alpha}\right)$  with lift coefficient at a Mach number of 0.25.

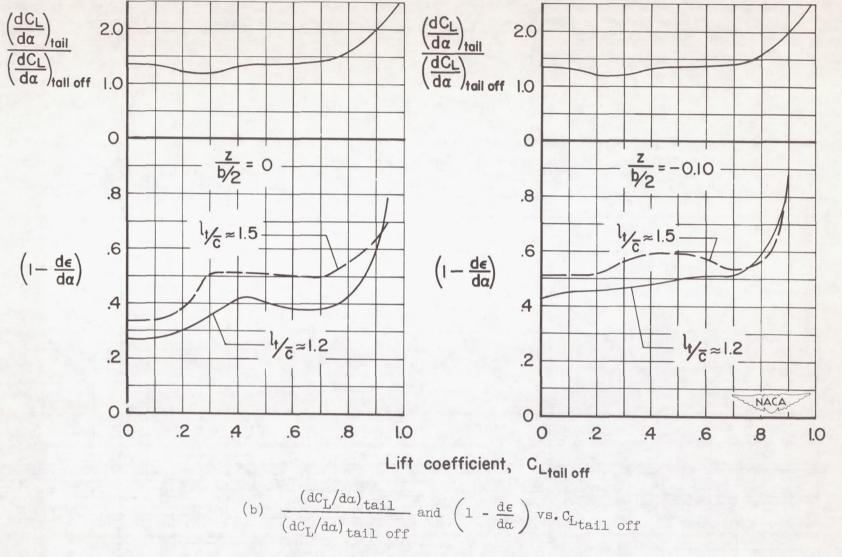


Figure 17. - Concluded.

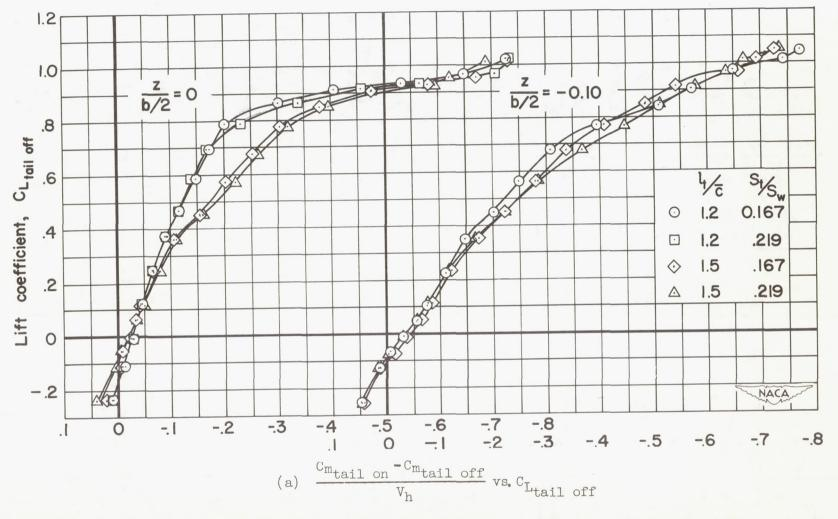
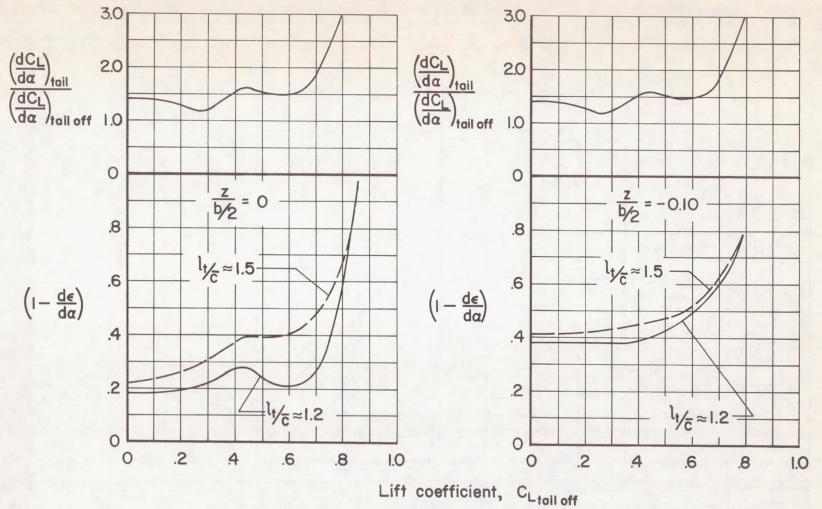


Figure 18.- The variations of the pitching-moment coefficient due to the horizontal tail and of the factors  $\frac{(dC_L/d\alpha)_{tail}}{(dC_L/d\alpha)_{tail}} \text{ and } \left(1-\frac{d\varepsilon}{d\alpha}\right) \text{ with lift coefficient at a Mach number of 0.80.}$ 



(b)  $\frac{(dC_L/d\alpha)_{tail}}{(dC_L/d\alpha)_{tail}}$  and  $\left(1 - \frac{d\epsilon}{d\alpha}\right)$  vs. $C_{Ltail}$  off

Figure 18.- Concluded.

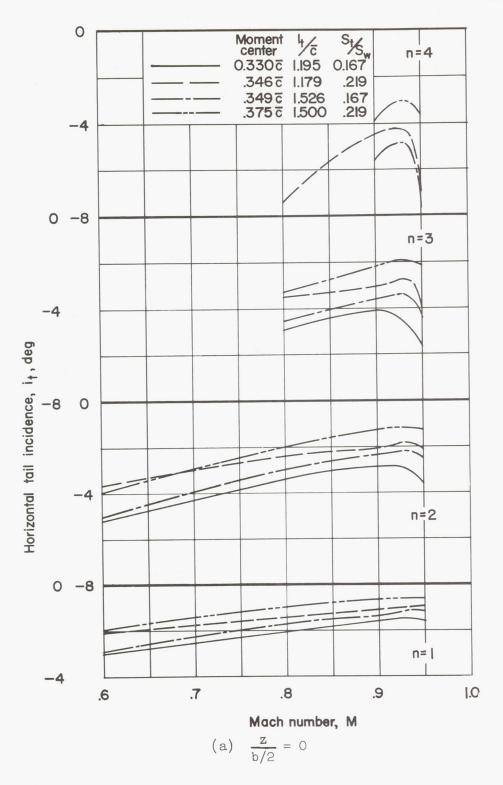
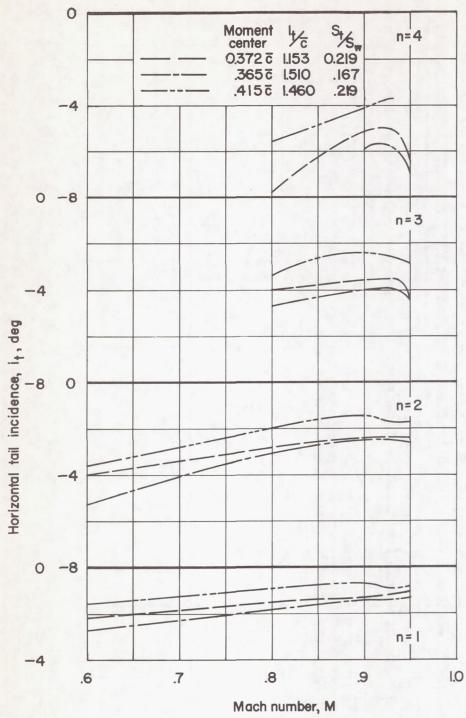


Figure 19.- The variation of tail incidence with Mach number for several normal acceleration factors at an altitude of 30,000 ft and a wing loading of 60 lb/ft $^2$ .



(b)  $\frac{z}{b/2} = -0.10$ 

Figure 19.- Concluded.

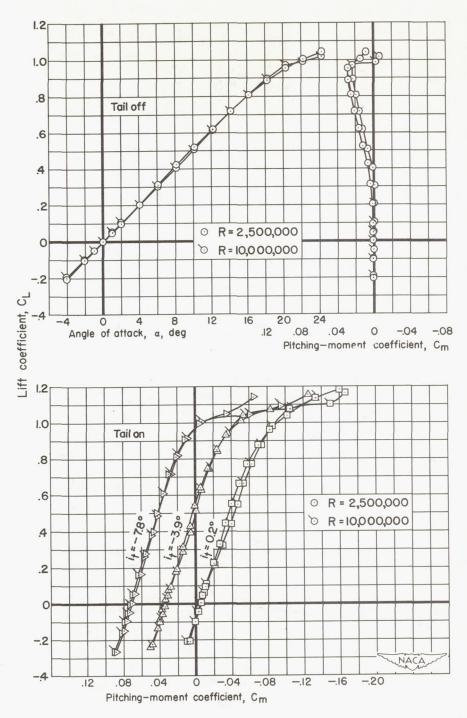


Figure 20.- The effect of Reynolds number on the lift and pitching-moment characteristics at a Mach number of 0.25. Wing and horizontal tail on the fuselage center line. Moment center at 0.349 $\bar{c}$ ,  $l_t/\bar{c}$  = 1.526,  $S_t/S_W$  = 0.167.

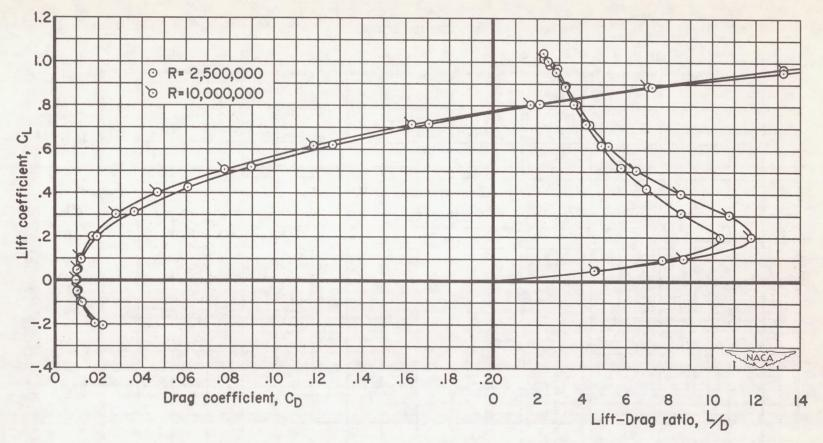


Figure 21.- The effect of Reynolds number on the drag characteristics of the wing-fuse lage combination with the wing in the mid position. M = 0.25.

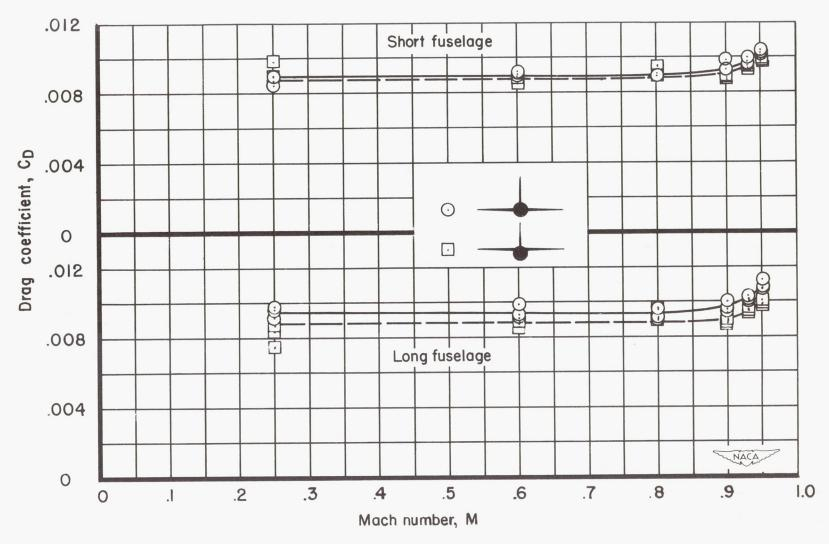
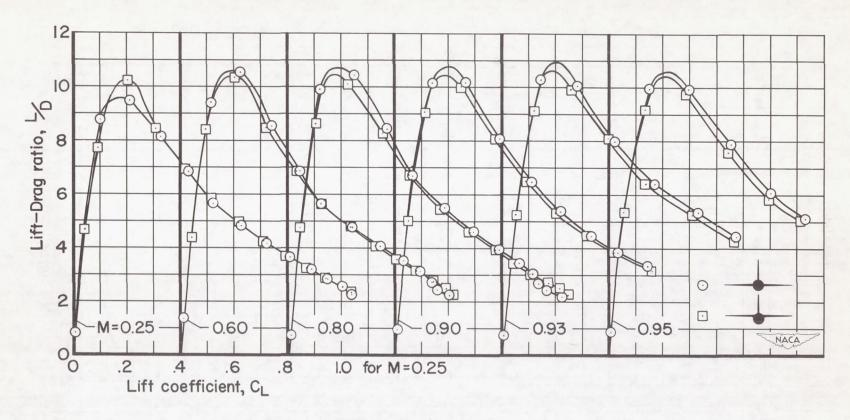
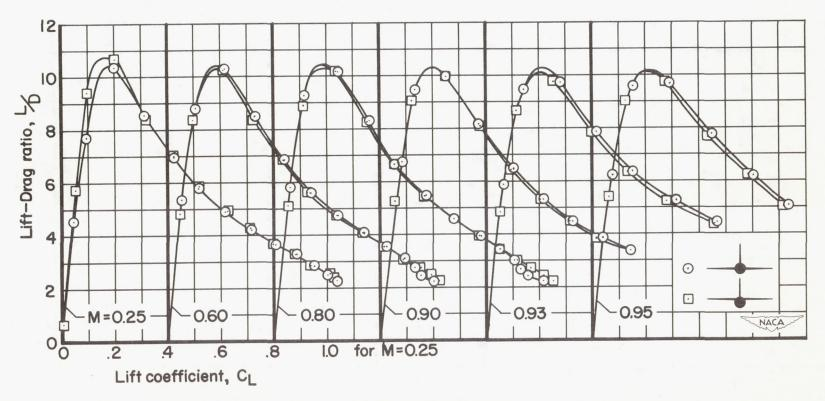


Figure 22.- Variation of the tail-off minimum drag coefficient with Mach number.



(a) Short fuselage.

Figure 23.- The variation of the tail-off lift-drag ratios with lift coefficient.



(b) Long fuselage.

Figure 23.- Concluded.

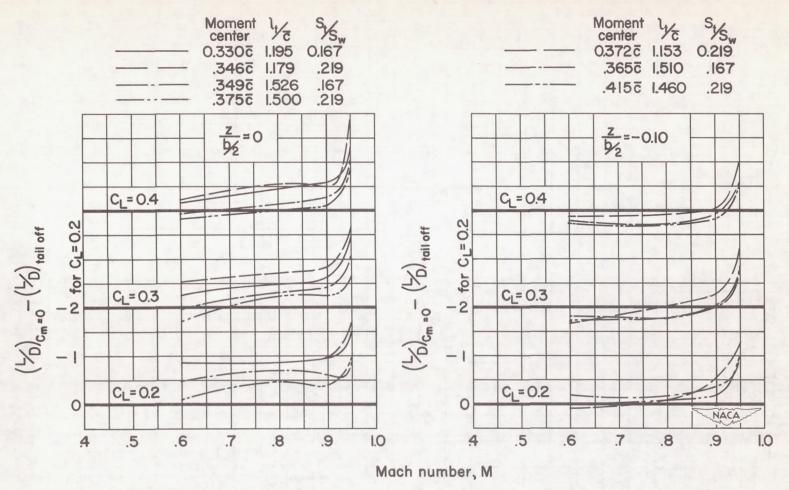


Figure 24.- The increment in lift-drag ratio due to balancing the model with a horizontal tail as evaluated from the measured lift and drag coefficients.

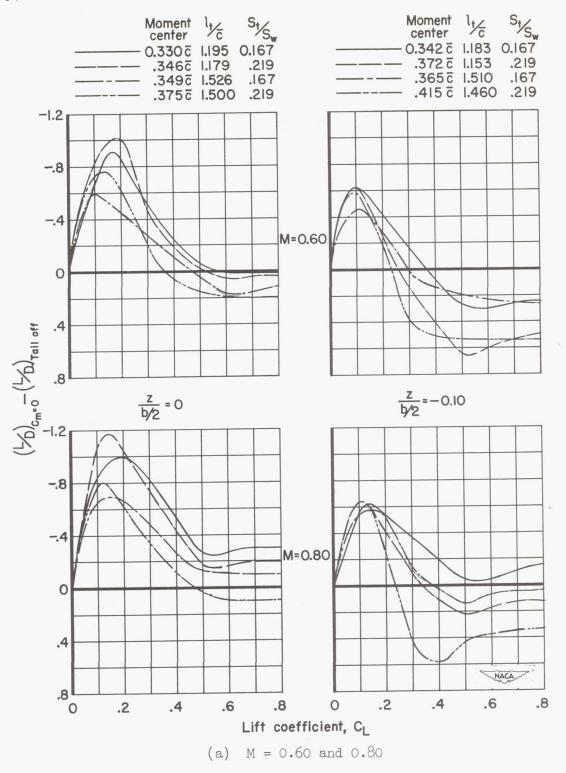
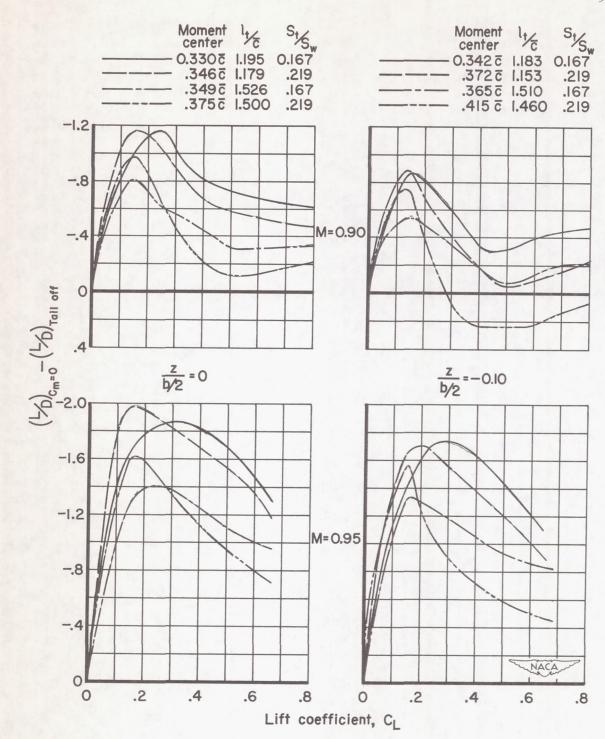


Figure 25.- The increment in lift-drag ratio due to balancing the model with a horizontal tail as calculated from the tail-off pitching-moment coefficients and  $\Delta^{C}\mathrm{D}_{Otail}$ .



(b) M = 0.90 and 0.95

Figure 25. - Concluded.